

# Supernova 2012aw - a high-energy clone of archetypal type IIP SN 1999em

Subhash Bose<sup>1\*</sup>, Brijesh Kumar<sup>1</sup>, Firoza Sutaria<sup>2</sup>, Brajesh Kumar<sup>1,3</sup>, Rupak Roy<sup>1</sup>, V. K. Bhatt<sup>1</sup>, S. B. Pandey<sup>1</sup>, H. C. Chandola<sup>4</sup>, Ram Sagar<sup>1</sup>, Kuntal Misra<sup>1</sup>, Sayan Chakraborti<sup>5</sup>

<sup>1</sup>*Aryabhata Research Institute of Observational Sciences, Manora Peak, Nainital - 263 002, India.*

<sup>2</sup>*Indian Institute of Astrophysics, Block-II, Koramangala, Bangalore - 560034, India.*

<sup>3</sup>*Institut d'Astrophysique et de Géophysique, Université de Liège, Allée du 6 Août 17, Bât B5c, 4000 Liège, Belgium*

<sup>4</sup>*Department of Physics, D.S.B. Campus, Kumaun University, Nainital - 263 002, India.*

<sup>5</sup>*Institute for Theory and Computation, Harvard-Smithsonian Center for Astrophysics, 60 Garden Street, Cambridge, MA 02138, USA.*

Accepted 2013 May 10; Received 2013 April 27

## ABSTRACT

We present densely-sampled *UBVRI/griz* photometric and low-resolution (6–10Å) optical spectroscopic observations from 4 to 270 days after explosion of a newly discovered type II SN 2012aw in a nearby ( $\sim 9.9$  Mpc) galaxy M95. The light-curve characteristics of apparent magnitudes, colors, bolometric luminosity and the presence and evolution of prominent spectral features are found to have striking similarity with the archetypal IIP SNe 1999em, 1999gi and 2004et. The early time observations of SN 2012aw clearly detect minima in the light-curve of *V*, *R* and *I* bands near 37 days after explosion and this we suggest to be an observational evidence for emergence of recombination phase. The mid-plateau  $M_V$  magnitude ( $-16.67 \pm 0.04$ ) lies in between the bright ( $\sim -18$ ) and subluminal ( $\sim -15$ ) IIP SNe. The mass of nickel is  $0.06 \pm 0.01 M_{\odot}$ . The SYNOW modelling of spectra indicate that the value and evolution of photospheric velocity is similar to SN 2004et, but about  $\sim 600 \text{ km s}^{-1}$  higher than that of SNe 1999em and 1999gi at comparable epochs. This trend is more apparent in the line velocities of  $H\alpha$  and  $H\beta$ . A comparison of ejecta velocity properties with that of existing radiation-hydrodynamical simulations indicate that the energy of explosion lies in the range  $1\text{--}2 \times 10^{51}$  ergs; a further comparison of nebular phase [O I] doublet luminosity with SNe 2004et and 1987A indicate that the mass of progenitor star is about  $14\text{--}15 M_{\odot}$ . The presence of high-velocity absorption features in the mid-to-late plateau and possibly in early phase spectra show signs of interaction between ejecta and the circumstellar matter; being consistent with its early-time detection at X-ray and radio wavebands.

**Key words:** supernovae: general – supernovae: individual: SN 2012aw, SN 1999em, SN 1999gi, SN 2004et – galaxies: individual: NGC 3551

## 1 INTRODUCTION

Early-time optical spectra of supernovae (SNe) showing strong Balmer lines of H are classified as type II, whereas SNe I show no H lines. Many sub-types have been introduced (Filippenko 1997) and in IIP, the optical light curve remains constant for about hundred days (called the plateau

phase) and then decays exponentially, while both IIL and IIB are characterized by linear decline in the light curves after reaching maxima at about twenty days after explosion (Arcavi et al. 2012). The spectra of all these types show strong P-Cygni line profiles, while the type IIB has weak H features initially and at later phases develop prominent He features similar to the type Ib SNe. Type IIn events show narrow width of H emission lines (Pastorello et al. 2002) which is indicative of interaction between the SN ejecta and

\* e-mail: email@subhashbose.com, bose@aries.res.in

the dense circumstellar medium. In addition, there are peculiar type II events such as SN 1987A which are characterized by long rise time of their light curve (Utrobin & Chugai 2011; Pastorello et al. 2012).

Type II SNe are widely recognized as end stages of massive ( $\gtrsim 8 M_{\odot}$ ) zero-age main-sequence stars which end up as core collapse explosions and having retained significant amount of H envelope before explosion (Burrows 2013). The observed properties derived from the light-curve and spectra of SNe provide important clues to the understanding of explosion mechanisms as well as to the nature of progenitor stars (Smartt et al. 2009). The plateau phase of IIP SNe is sustained by cooling down of the shock-heated expanding ejecta by recombination of H while the post-plateau light curve is powered by the radioactive decay of  $^{56}\text{Co}$  into  $^{56}\text{Fe}$ , which in turn depend upon the amount of  $^{56}\text{Ni}$  synthesized during explosion. The observed properties of IIP SNe differ greatly (Hamuy 2003; Smartt et al. 2009), for example, the mid-plateau bolometric luminosity vary by an order of magnitude from  $\sim 10^{42.5} \text{ erg s}^{-1}$  for archetypal IIP SN 2004et to  $\sim 10^{41.5} \text{ erg s}^{-1}$  for under luminous SN 2005cs. The class of subluminescent events (Pastorello et al. 2004, 2009) are also accompanied by lower ejecta velocity during plateau ( $\sim 1000 \text{ km s}^{-1}$ ) and lower luminosity in the light curve tail owing to small yield of  $^{56}\text{Ni}$  ( $\sim 2 - 5 \times 10^{-3} M_{\odot}$ ), in comparison to the normal luminosity IIP SNe 1999em, 2004et with velocities ( $\sim 5000 \text{ km s}^{-1}$ ) and the mass of  $^{56}\text{Ni}$  ( $\sim 0.1 M_{\odot}$ ). The subluminescent IIP events are associated with O-Ne-Mg core originating from lower-mass progenitors ( $8-10 M_{\odot}$ ), while the normal ones originate from iron-core collapse of massive ( $> 10 M_{\odot}$ ) progenitors (Fraser et al. 2011; Janka 2012). However, there are cases, i.e. SN 2008in (Roy et al. 2011) and SN 2009js (Gandhi et al. 2013), where a spectroscopically subluminescent IIP event show light curve properties similar to a normal luminosity event.

The stellar evolution models suggest that type IIP SNe originate from red supergiants having initial masses between  $9-25 M_{\odot}$  having an upper mass cut of  $32 M_{\odot}$  for solar metallicity stars (Heger et al. 2003), however, the observational constraints are ambiguous and the mass of progenitors recovered from the analysis of pre-explosion archival HST images for 20 IIP SNe lie in the range  $9-17 M_{\odot}$  (Smartt et al. 2009) while the hydrodynamical modelling of light curves for a handful of well studied IIP SNe indicate that they primarily originate from  $15-25 M_{\odot}$  progenitors (Utrobin & Chugai 2009; Bersten et al. 2011). Some of the problems in inferring physical properties are the lack of good quality data for nearby SNe.

SN 2012aw was discovered on March 16.9, 2012 by Fagotti et al. (2012) in the nearby galaxy M95 ( $\sim 10 \text{ Mpc}$ ) at R-band magnitude of 15. The first non-detection is reported on March 15.27 (Poznanski et al. 2012a) to a  $3\sigma$  limit of  $R \sim 20.7$ . Thus, we adopt March 16.1, 2012 (JD=2456002.6  $\pm$  0.8 days) as the time of explosion (0 d) through out the paper. The spectra obtained at 2d by Munari et al. (2012) showed a featureless blue continuum while the subsequent spectra at later phases by Itoh et al. (2012); Siviero et al. (2012) identifies the event as young type IIP. The ultraviolet follow-up observations with UVOT/Swift is done by Bayless et al. (2013) and similar to the optical, they report emergence of plateau in the UV light curve after 27d. The analysis of pre-explosion

archival HST images of M95 in the vicinity of SN 2012aw, by two independent group of researchers indicate that the progenitor was a red supergiant with masses in the range  $14-26 M_{\odot}$  (Fraser et al. 2012) and  $15-20 M_{\odot}$  (Van Dyk et al. 2012) respectively. However, by accounting for appropriate extinction laws to the circumstellar and interstellar dust, Kochanek et al. (2012) determine that the luminosity of the progenitor star lie between 4.8 to 5.0 dex in solar units and the mass was less than  $15 M_{\odot}$ . SN 2012aw was also detected in X-rays observations with swift/XRT by Immler & Brown (2012) and in radio observations by Stockdale et al. (2012); Yadav et al. (2012) indicating interaction of ejecta with the circumstellar material. The early time (17d) optical spectropolarimetric observations with 8-m ESO VLT by Leonard et al. (2012) finds continuum polarization at the level of 0.3% implying substantial asymmetries in the outer ejecta of SN 2012aw.

In this work, we present results from optical photometric (*UBVRI* and/or *griz*) photometric follow-up observations at 45 phases during 4d to 269d and low-resolution optical spectroscopic observations at 14 phases during 7d to 270d of SN 2012aw. The paper is organized as follows. In §2.1 and §2.2, we present the photometric and spectroscopic observations respectively and a brief description of light curves and spectra. Determination of reddening and extinction is given in §3. In §4, we analyze light and color curves, derive bolometric light-curves and estimate mass of nickel. In §5, we study spectra, evolution of spectral features, *SYNOW* modelling and derive velocity of hydrogen envelope and the photosphere. The characteristics of explosion is described in §6 and conclusions are presented in §7.

We adopt the distance to the host galaxy M95 as  $9.9 \pm 0.1 \text{ Mpc}$  which is a weighted mean of three most reliable redshift-independent distance measurements in the literature, i.e.  $10 \pm 0.40 \text{ Mpc}$  by Freedman et al. (2001) using cepheids;  $9.86 \pm 0.14 \text{ Mpc}$  by Russell (2002) using Tully-Fisher method and  $9.83 \pm 0.13 \text{ Mpc}$  by Bose & Kumar (2013) using SN Expanding photosphere method. SN 2012aw occurred in the outskirts of the host galaxy at a deprojected distance of 6.8 kpc and the oxygen abundance ( $12 + \log[\text{O}/\text{H}]$ ) of the galactic ISM at the position of SN is estimated as  $8.8 \pm 0.1$  from the radial metallicity gradient relation in M95 given by Pilyugin et al. (2006) and this value is close to the solar abundance for oxygen of 8.65 (Asplund et al. 2009). Some basic properties of the host galaxy and SN 2012aw is listed in Table 1.

## 2 OBSERVATION AND DATA REDUCTION

### 2.1 Photometry

The broadband photometric data in *UBVRI* Johnson-Cousins and *griz* SDSS systems are collected using the 104-cm Sampurnanand Telescope (ST) at Manora Peak, Nainital and the 130-cm Devasthal Fast Optical Telescope (DFOT) at Devasthal, Nainital. Both the telescopes are operated by the Aryabhata Research Institute of Observational sciences, India (Sagar et al. 2013). The 104-cm ST is equipped with a  $2\text{k} \times 2\text{k}$  liquid-nitrogen cooled CCD camera having square pixels of  $24 \mu\text{m}$ ; and with a plate scale of  $0''.37$  per pixel, the CCD covers a square field-of-view of about  $13'$  on a side in

**Table 1.** Properties of the host galaxy NGC 3351 and SN 2012aw.

Parameters	Value	Ref. <sup>a</sup>
<b>NGC 3351:</b>		
Type	Sb	1
RA (J2000)	$\alpha = 10^{\text{h}}43^{\text{m}}57^{\text{s}}.67$	1
DEC (J2000)	$\delta = 11^{\circ}42'13''.0$	1
Abs. Magnitude	$M_B = -20.36$ mag	1
Distance	$D = 9.9 \pm 0.1$ Mpc	§1
Scale	$1'' \sim 48$ pc, $1' \sim 2.9$ kpc	
Distance modulus	$\mu = 29.97 \pm 0.03$	
Apparent radius	$r_{25} = 3'.6$ ( $\sim 10.5$ kpc)	1
Inclination angle	$\Theta_{\text{inc}} = 54.6^{\circ}$	1
Position angle	$\Theta_{\text{maj}} = 9.9^{\circ}$	1
Heliocentric Velocity	$v_{\text{helio}} = 778 \pm 2$ km s <sup>-1</sup>	1
<b>SN 2012aw:</b>		
RA (J2000)	$\alpha = 10^{\text{h}}43^{\text{m}}53^{\text{s}}.73$	2
DEC (J2000)	$\delta = 11^{\circ}40'17''.9$	
Galactocentric Location	58'' W, 115'' S	
Deprojected radius	$r_{\text{SN}} = 139'.1$ ( $\sim 6.75$ kpc)	
Time of explosion	$t_0 = 16.1$ March 2012 (UT) (JD 2456002.59)	§1
Reddening	$E(B - V) = 0.074 \pm 0.008$	§3

<sup>a</sup> (1) HyperLEDA - <http://leda.univ-lyon1.fr>;  
 (2) Van Dyk et al. (2012)

the sky. While operating at 27 kHz, the gain and readout noise of the CCD are  $10e^-$  per analog-to-digital unit and  $5.3e^-$  respectively. The 130-cm DFOT is equipped with a  $2k \times 2k$  Peltier-cooled CCD camera having a pixel size of  $13.5 \mu\text{m}$ ; and with a plate scale of  $0''.54$  per pixel, the CCD covers a square field-of-view of  $18'$  on a side. The CCD was operated at 31 kHz speed with readout noise of  $2.5e^-$  – a detailed technical description and performance of this camera can be found elsewhere (Sagar et al. 2012). A binning of  $2 \times 2$  is used in CCDs wherever required to improve the signal-to-noise ratio. At 104-cm ST, we had *UBVRI* while at 130-cm, we had *BVR* as well as *griz* filters. A typical exposure time of 300s were given for *U* and *B* filters while 80-200s were given for remaining filters. For V-band, the full width at half maximum (FWHM) of the stellar point spread function (PSF) varied between  $2''.1$  to  $3''.5$ , with a median value of  $2''.6$ . In addition to the target exposures, several bias and twilight flat frames are also obtained for calibration purpose.

The bias subtraction, flat fielding, cosmic ray removal, alignment and determination of mean FWHM and ellipticity for each object frames are done using the standard tasks available in the data reduction softwares IRAF<sup>1</sup> and

<sup>1</sup> IRAF stands for Image Reduction and Analysis Facility distributed by the National Optical Astronomy Observatories which is operated by the Association of Universities for research in Astronomy, Inc. under co-operative agreement with the National Science Foundation.

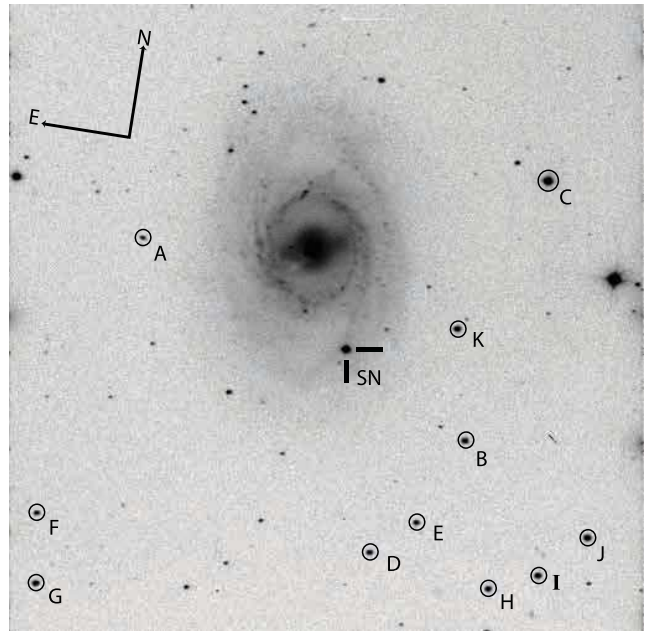


**Figure 1.** SN 2012aw in NGC 3351. The V-band image taken from 104-cm ST covering an area of about  $13' \times 13'$  is shown. The location of SN and local standard stars are marked.

DAOPHOT<sup>2</sup>. Whenever multiple frames are available, the photometry is performed on co-added frames. As the location of SN is fairly isolated from the galaxy center and it lies on a smooth and faint galaxy background (see Fig. 1), we chose to perform aperture photometry; and an aperture radius equal to the mean FWHM of a given frame and a 10 pixel wide sky annulus at 6 FWHM radius were chosen. This whole scheme of aperture photometry is achieved using standalone version of DAOPHOT subroutines. The differential instrumental magnitude for each filter was generated using DAOMASTER task.

In order to calibrate instrumental magnitude of SN 2012aw, the Landolt (2009) standard fields PG 1323, PG 1525 and PG 1633 were observed on 22nd March 2012 in *UBVRI* filters with the 104-cm ST under photometric night conditions viz. transparent sky, FWHM seeing in *V*  $\sim 2''$ . The observations of standard fields were taken at five locations covering airmass from 1.06 to 2.36. The SN field is also observed on the same night. The data reduction of SN and Landolt fields are done using profile fitting technique and the instrumental magnitudes were converted into standard system following least-square linear regression procedures outlined in Stetson (1992), in which zero-points, color coefficients and the atmospheric extinction coefficients are fitted simultaneously for 17 stars having *V* magnitude from 12.0 to 16.4 and *B - V* from  $-0.22$  to  $1.14$  mag. The root-mean-squared (RMS) scatter between the transformed and the standard magnitudes of Landolt stars is found to be  $\sim 0.04$  mag in *U*,  $0.02$  mag in *B* and  $0.01$  mag in *VRI*. The transformation coefficients were used to generate local standard stars in the field of SN 2012aw observed on the same night and a set of 11 stars with *V* range from 12 to 17 mag and *B - V* range of  $0.36$  to  $1.06$  mag were selected.

<sup>2</sup> DAOPHOT stands for Dominion Astrophysical Observatory Photometry (Stetson 1987)

**Table 2.** Identification number (ID), coordinates ( $\alpha, \delta$ ) and calibrated magnitudes of stable secondary standard stars in the field of SN 2012aw. The field of SN 2012aw was calibrated using Landolt standards observed on the night of 22nd March 2012. The quoted errors in magnitude include both photometric and calibration errors and it denote  $1\sigma$  uncertainty.

Star ID	$\alpha_{J2000}$ (h m s)	$\delta_{J2000}$ ( $^{\circ}$ $'$ $''$ )	$U$ (mag)	$B$ (mag)	$V$ (mag)	$R$ (mag)	$I$ (mag)
A	10:44:11.82	+11:41:54.5	18.168 $\pm$ 0.078	17.650 $\pm$ 0.045	16.775 $\pm$ 0.057	16.316 $\pm$ 0.024	15.841 $\pm$ 0.017
B	10:43:42.70	+11:38:51.1	15.801 $\pm$ 0.024	15.611 $\pm$ 0.008	14.897 $\pm$ 0.011	14.493 $\pm$ 0.013	14.049 $\pm$ 0.016
C	10:43:39.17	+11:44:21.3	13.774 $\pm$ 0.014	12.882 $\pm$ 0.007	11.878 $\pm$ 0.026	11.358 $\pm$ 0.035	10.866 $\pm$ 0.035
D	10:43:49.09	+11:36:17.4	16.277 $\pm$ 0.024	16.179 $\pm$ 0.012	15.522 $\pm$ 0.017	15.139 $\pm$ 0.021	14.748 $\pm$ 0.019
E	10:43:45.65	+11:37:02.8	16.804 $\pm$ 0.037	16.453 $\pm$ 0.012	15.668 $\pm$ 0.013	15.243 $\pm$ 0.016	14.817 $\pm$ 0.022
F	10:44:17.02	+11:36:02.1	16.540 $\pm$ 0.026	16.760 $\pm$ 0.012	16.399 $\pm$ 0.014	16.123 $\pm$ 0.026	15.795 $\pm$ 0.016
G	10:44:16.18	+11:34:37.0	16.277 $\pm$ 0.031	15.687 $\pm$ 0.015	14.851 $\pm$ 0.014	14.397 $\pm$ 0.019	13.966 $\pm$ 0.018
H	10:43:38.86	+11:35:56.5	16.160 $\pm$ 0.023	15.919 $\pm$ 0.012	15.207 $\pm$ 0.016	14.818 $\pm$ 0.020	14.453 $\pm$ 0.023
I	10:43:34.96	+11:36:22.2	15.746 $\pm$ 0.022	15.494 $\pm$ 0.009	14.787 $\pm$ 0.012	14.406 $\pm$ 0.025	13.966 $\pm$ 0.016
J	10:43:31.33	+11:37:17.7	15.954 $\pm$ 0.018	14.955 $\pm$ 0.006	13.896 $\pm$ 0.013	13.300 $\pm$ 0.025	12.712 $\pm$ 0.016
K	10:43:44.75	+11:41:04.4	15.190 $\pm$ 0.020	15.328 $\pm$ 0.009	14.944 $\pm$ 0.009	14.727 $\pm$ 0.012	14.467 $\pm$ 0.014

**Table 3.** Photometric evolution of SN 2012aw. Errors denote  $1\sigma$  uncertainty.

UT Date (yy/mm/dd)	JD 2456000+	Phase <sup>a</sup> (day)	$U$ (mag)	$B$ (mag)	$V$ (mag)	$R$ (mag)	$I$ (mag)	Tel <sup>b</sup>	Seeing <sup>c</sup> ( $''$ )
2012-03-19.82	006.32	4	12.671 $\pm$ 0.042	13.504 $\pm$ 0.021	13.574 $\pm$ 0.017	13.463 $\pm$ 0.018	13.433 $\pm$ 0.025	ST	2.6
2012-03-20.80	007.30	5	12.582 $\pm$ 0.042	13.492 $\pm$ 0.021	13.478 $\pm$ 0.017	13.372 $\pm$ 0.018	13.325 $\pm$ 0.025	ST	2.3
2012-03-21.81	008.31	6	12.517 $\pm$ 0.042	13.457 $\pm$ 0.021	13.420 $\pm$ 0.012	13.300 $\pm$ 0.018	13.258 $\pm$ 0.018	ST	2.0
2012-03-22.76	009.26	7	12.599 $\pm$ 0.042	13.415 $\pm$ 0.021	13.380 $\pm$ 0.017	13.262 $\pm$ 0.018	13.239 $\pm$ 0.025	ST	2.0
2012-03-24.84	011.34	9	12.652 $\pm$ 0.042	13.394 $\pm$ 0.021	13.340 $\pm$ 0.017	13.175 $\pm$ 0.018	13.132 $\pm$ 0.025	ST	1.9
2012-03-25.78	012.28	10	12.676 $\pm$ 0.043	13.411 $\pm$ 0.021	13.328 $\pm$ 0.017	13.192 $\pm$ 0.014	13.130 $\pm$ 0.025	ST	2.3
2012-04-01.63	019.13	17	13.010 $\pm$ 0.042	13.567 $\pm$ 0.021	13.318 $\pm$ 0.017	13.089 $\pm$ 0.018	12.990 $\pm$ 0.025	ST	2.2
2012-04-07.63	025.13	23	13.627 $\pm$ 0.043	13.756 $\pm$ 0.021	13.325 $\pm$ 0.017	13.073 $\pm$ 0.018	12.923 $\pm$ 0.025	ST	2.2
2012-04-09.74	027.24	25	13.909 $\pm$ 0.042	13.875 $\pm$ 0.021	13.351 $\pm$ 0.017	13.086 $\pm$ 0.018	12.950 $\pm$ 0.025	ST	2.3
2012-04-12.71	030.21	28	14.199 $\pm$ 0.042	14.000 $\pm$ 0.021	13.366 $\pm$ 0.017	13.111 $\pm$ 0.018	12.940 $\pm$ 0.025	ST	2.4
2012-04-19.65	037.15	35	14.788 $\pm$ 0.043	14.228 $\pm$ 0.021	13.439 $\pm$ 0.017	13.140 $\pm$ 0.018	12.918 $\pm$ 0.025	ST	2.5
2012-04-21.61	039.11	37	14.905 $\pm$ 0.043	14.284 $\pm$ 0.021	13.468 $\pm$ 0.017	13.151 $\pm$ 0.018	12.895 $\pm$ 0.018	ST	2.9
2012-04-22.82	040.32	38	—	—	13.493 $\pm$ 0.017	13.135 $\pm$ 0.018	12.899 $\pm$ 0.052	ST	2.7
2012-04-25.75	043.25	41	15.189 $\pm$ 0.044	14.392 $\pm$ 0.021	13.463 $\pm$ 0.017	13.124 $\pm$ 0.018	12.851 $\pm$ 0.025	ST	2.1
2012-04-29.70	047.20	45	15.377 $\pm$ 0.050	14.466 $\pm$ 0.021	13.487 $\pm$ 0.017	13.126 $\pm$ 0.018	12.836 $\pm$ 0.025	ST	2.8
2012-05-01.61	049.11	47	15.455 $\pm$ 0.057	14.491 $\pm$ 0.025	13.725 $\pm$ 0.024	13.115 $\pm$ 0.023	12.887 $\pm$ 0.035	ST	2.9
2012-05-04.63	052.13	50	15.552 $\pm$ 0.089	—	13.439 $\pm$ 0.018	13.115 $\pm$ 0.018	12.776 $\pm$ 0.055	ST	2.1
2012-05-06.62	054.12	52	—	14.574 $\pm$ 0.021	13.471 $\pm$ 0.017	13.116 $\pm$ 0.018	12.790 $\pm$ 0.052	ST	2.4
2012-05-08.61	056.11	54	—	—	13.526 $\pm$ 0.018	13.113 $\pm$ 0.019	12.812 $\pm$ 0.026	ST	2.7
2012-05-09.61	057.11	55	15.802 $\pm$ 0.067	14.688 $\pm$ 0.024	13.494 $\pm$ 0.017	13.088 $\pm$ 0.018	12.775 $\pm$ 0.025	ST	2.9
2012-05-11.65	059.15	57	—	14.518 $\pm$ 0.022	13.534 $\pm$ 0.017	13.085 $\pm$ 0.018	—	DFOT	3.1
2012-05-13.68	061.18	59	16.049 $\pm$ 0.059	14.697 $\pm$ 0.021	13.539 $\pm$ 0.017	13.097 $\pm$ 0.018	12.804 $\pm$ 0.025	ST	2.6
2012-05-14.69	062.19	60	16.133 $\pm$ 0.068	14.711 $\pm$ 0.022	13.566 $\pm$ 0.017	13.139 $\pm$ 0.018	12.797 $\pm$ 0.025	ST	2.6
2012-05-17.64	065.14	63	16.239 $\pm$ 0.049	14.771 $\pm$ 0.021	13.556 $\pm$ 0.017	13.102 $\pm$ 0.018	12.774 $\pm$ 0.025	ST	2.8
2012-05-24.63	072.13	70	16.424 $\pm$ 0.089	14.817 $\pm$ 0.021	13.571 $\pm$ 0.017	13.106 $\pm$ 0.018	12.787 $\pm$ 0.025	ST	3.1
2012-05-27.66	075.16	73	16.577 $\pm$ 0.144	14.882 $\pm$ 0.022	13.596 $\pm$ 0.018	13.118 $\pm$ 0.018	12.778 $\pm$ 0.025	ST	2.9
2012-05-27.65	075.15	73	—	14.611 $\pm$ 0.023	13.596 $\pm$ 0.012	13.110 $\pm$ 0.018	—	DFOT	2.8
2012-05-28.63	076.13	74	—	14.609 $\pm$ 0.025	13.637 $\pm$ 0.018	13.115 $\pm$ 0.018	—	DFOT	3.1
2012-05-30.65	078.15	76	—	14.872 $\pm$ 0.031	13.627 $\pm$ 0.018	13.126 $\pm$ 0.018	12.786 $\pm$ 0.025	ST	3.8
2012-06-06.64	085.14	83	16.840 $\pm$ 0.061	14.990 $\pm$ 0.021	13.687 $\pm$ 0.017	13.127 $\pm$ 0.018	12.804 $\pm$ 0.018	ST	3.4
2012-06-09.62	088.12	86	17.010 $\pm$ 0.062	15.042 $\pm$ 0.022	13.664 $\pm$ 0.017	13.174 $\pm$ 0.018	12.828 $\pm$ 0.025	ST	2.5
2012-06-11.63	090.13	88	16.886 $\pm$ 0.052	15.057 $\pm$ 0.021	13.670 $\pm$ 0.017	13.159 $\pm$ 0.018	12.815 $\pm$ 0.025	ST	2.8
2012-06-16.66	095.16	93	—	14.694 $\pm$ 0.029	13.727 $\pm$ 0.018	13.206 $\pm$ 0.013	—	DFOT	3.3
2012-06-25.65	104.15	102	—	15.231 $\pm$ 0.029	13.873 $\pm$ 0.022	13.361 $\pm$ 0.023	12.995 $\pm$ 0.031	ST	3.7
2012-06-27.63	106.13	104	16.979 $\pm$ 0.219	15.158 $\pm$ 0.018	13.824 $\pm$ 0.017	13.296 $\pm$ 0.018	12.947 $\pm$ 0.025	ST	3.7
2012-10-16.96	217.46	215	—	17.526 $\pm$ 0.083	16.577 $\pm$ 0.025	15.794 $\pm$ 0.020	—	DFOT	3.5
2012-10-17.96	218.46	216	—	17.657 $\pm$ 0.053	16.617 $\pm$ 0.024	15.823 $\pm$ 0.014	—	DFOT	3.5
2012-10-23.98	224.48	222	—	18.069 $\pm$ 0.361	16.918 $\pm$ 0.366	—	15.413 $\pm$ 0.059	ST	3.4
2012-10-24.97	225.47	223	—	18.033 $\pm$ 0.026	16.711 $\pm$ 0.019	15.832 $\pm$ 0.019	15.368 $\pm$ 0.026	ST	2.2
2012-10-26.97	227.47	225	—	18.106 $\pm$ 0.023	16.730 $\pm$ 0.019	15.860 $\pm$ 0.019	15.389 $\pm$ 0.026	ST	2.7
2012-10-29.99	230.49	228	—	—	16.667 $\pm$ 0.015	—	—	ST	1.7
2012-10-30.98	231.48	229	19.551 $\pm$ 0.361	18.088 $\pm$ 0.038	16.765 $\pm$ 0.020	15.899 $\pm$ 0.014	15.447 $\pm$ 0.025	ST	1.8
2012-11-02.97	234.47	232	—	18.163 $\pm$ 0.030	16.803 $\pm$ 0.020	15.949 $\pm$ 0.011	15.454 $\pm$ 0.026	ST	2.0
2012-11-04.96	236.46	234	—	18.126 $\pm$ 0.030	16.841 $\pm$ 0.016	15.975 $\pm$ 0.020	15.456 $\pm$ 0.026	ST	2.0
2012-11-07.97	239.47	237	—	18.278 $\pm$ 0.078	16.721 $\pm$ 0.046	15.955 $\pm$ 0.031	15.454 $\pm$ 0.040	ST	2.2
2012-11-10.95	242.45	240	—	17.850 $\pm$ 0.051	16.911 $\pm$ 0.022	15.992 $\pm$ 0.019	—	DFOT	2.9
2012-11-11.94	243.44	241	—	17.875 $\pm$ 0.051	16.963 $\pm$ 0.021	15.996 $\pm$ 0.019	—	DFOT	3.0
2012-11-16.98	248.48	246	20.291 $\pm$ 0.239	18.264 $\pm$ 0.019	16.908 $\pm$ 0.014	16.039 $\pm$ 0.019	15.586 $\pm$ 0.019	ST	2.0
2012-11-18.98	250.48	248	19.934 $\pm$ 0.153	18.289 $\pm$ 0.020	16.927 $\pm$ 0.018	16.054 $\pm$ 0.019	15.610 $\pm$ 0.026	ST	1.7
2012-11-25.95	257.45	255	19.821 $\pm$ 0.111	18.323 $\pm$ 0.018	17.011 $\pm$ 0.014	16.132 $\pm$ 0.019	15.709 $\pm$ 0.026	ST	1.9
2012-12-04.90	266.40	264	—	18.325 $\pm$ 0.060	17.051 $\pm$ 0.040	16.012 $\pm$ 0.036	15.726 $\pm$ 0.050	ST	2.0
2012-12-04.86	266.36	264	—	—	17.130 $\pm$ 0.071	—	—	DFOT	3.0
2012-12-09.02	270.52	268	—	18.415 $\pm$ 0.070	17.109 $\pm$ 0.022	16.225 $\pm$ 0.020	15.811 $\pm$ 0.026	ST	2.6
2012-12-09.98	271.48	269	20.166 $\pm$ 0.165	18.429 $\pm$ 0.022	17.113 $\pm$ 0.019	16.242 $\pm$ 0.019	15.837 $\pm$ 0.026	ST	2.2
			$g$ (mag)	$r$ (mag)	$i$ (mag)	$z$ (mag)			
2012-05-11.66	059.16	57	13.922 $\pm$ 0.031	13.242 $\pm$ 0.028	13.187 $\pm$ 0.021	13.185 $\pm$ 0.070	—	DFOT	3.1
2012-05-27.68	075.18	73	14.038 $\pm$ 0.031	13.259 $\pm$ 0.028	13.199 $\pm$ 0.021	13.164 $\pm$ 0.049	—	DFOT	2.8
2012-05-28.65	076.15	74	14.052 $\pm$ 0.031	13.269 $\pm$ 0.028	13.192 $\pm$ 0.021	13.172 $\pm$ 0.070	—	DFOT	3.1
2012-06-16.67	095.17	93	14.173 $\pm$ 0.031	13.326 $\pm$ 0.028	13.259 $\pm$ 0.021	13.192 $\pm$ 0.070	—	DFOT	3.3
2012-10-16.97	217.47	215	17.150 $\pm$ 0.033	15.948 $\pm$ 0.028	15.907 $\pm$ 0.022	15.376 $\pm$ 0.071	—	DFOT	3.5
2012-10-17.98	218.48	216	17.161 $\pm$ 0.033	15.971 $\pm$ 0.028	15.914 $\pm$ 0.022	15.399 $\pm$ 0.071	—	DFOT	3.5
2012-11-10.93	242.43	240	17.339 $\pm$ 0.033	16.171 $\pm$ 0.028	16.158 $\pm$ 0.022	15.570 $\pm$ 0.071	—	DFOT	2.9
2012-11-11									

These stars are identified in Fig. 1 and are listed in Table 2. The quoted errors include both photometric and calibration errors propagated in quadrature. The frame-to-frame photometric variability of these stars during 4d to 269d were found to lie within quoted uncertainties. Four of these stars are in common with the study of Henden et al. (2012) who provided calibrated *BVRI* magnitudes of 14 stars in  $20' \times 20'$  field of SN 2012aw. A comparison with their photometry gives a mean and RMS scatter of  $-0.04 \pm 0.04$ ,  $-0.01 \pm 0.03$ ,  $0.02 \pm 0.04$  and  $0.00 \pm 0.03$  mag respectively for *B*, *V*, *R* and *I*; indicating that the two photometric measurements are consistent within uncertainties. The magnitude of local standards in *griz* were taken from Lupton et al. 2005. The final photometry of SN 2012aw is given in Table 3.

## 2.2 Spectroscopy

During 7d to 270d, long-slit low-resolution spectra in the optical range were collected at 14 epochs; nine from 2m IUCAA Girawali Observatory (IGO) telescope and five from 2m Himalayan Chandra Telescope (HCT). Journal of spectroscopic observations are given in Table 4. Observations at 2m IGO have been carried out using IUCAA Faint Object Spectrograph and Camera (IFOSC) mounted at the cassegrain focus of f/10 reflector (Gupta et al. 2002; Chakraborty et al. 2005). Grisms 5 ( $\lambda \sim 0.33\text{-}0.63 \mu\text{m}$ ;  $\Delta\lambda \sim 8.8 \text{ \AA}$ ) and pair of grism 7 & 8 ( $\lambda \sim 0.38\text{-}0.83\mu\text{m}$ ;  $\Delta\lambda \sim 4 \text{ \AA}$ ) along with a slit width of  $1''.5$  are used to record spectra on  $2048 \times 2048$  E2V CCD with  $13.5 \mu\text{m}$  pixel size; having a gain of  $1.5 e^-$  per analog-to-digital unit (ADU) and readout noise of  $4 e^-$ . Calibration frames (bias, flat, HeNe arc) and spectrophotometric flux standard stars (Feige34, Hr4468 and Hz44) were observed on each night. Observations from 2m HCT have been carried out in similar fashion with HFOSC using pair of grisms 7&8 ( $\lambda \sim 0.38\text{-}0.84\mu\text{m}$ ;  $\Delta\lambda \sim 4 \text{ \AA}$ ) and a slit width of  $1''.92$ . For flux calibration, stars Feige66, Feige110 and Grw70d5824 are observed and FeAr and FeNe arcs are observed for wavelength calibrations.

Spectroscopic data reduction was done under IRAF environment. Bias and flat fielding were performed on each frames. Cosmic ray rejection on each frame were done using Laplacian kernel detection algorithm for spectra, L.A.Cosmic (van Dokkum 2001). One-dimensional spectra were extracted using *apall* task which is based on optimal extraction algorithm by Horne (1986). Wavelength calibration were performed using *identify* task and about 15-18 emission lines of HeNe (for IGO) or FeNe and FeAr (for HCT) were used to find dispersion solution. The position of OI emission skyline at  $5577\text{\AA}$  was used to check the wavelength calibration and deviations were found to lie between  $0.3$  to  $5.5\text{\AA}$  and this was corrected by applying a linear shift in wavelength. The instrumental FWHM resolution of 2m IGO spectra as measured from OI5577 $\text{\AA}$  emission skyline was found to lie between  $\sim 6$  to  $12\text{\AA}$  ( $\sim 317 - 671 \text{ km s}^{-1}$ ) and that of 2m HCT was found to lie between  $\sim 8$  to  $10\text{\AA}$ .

The flux calibration of wavelength-calibrated spectra was done using *standard*, *sensfunc* and *calibrate* tasks. We used spectrophotometric standard fluxes from Oke (1990); Hamuy et al. (1994) and the spectral extinction coefficients from Stalin et al. (2008); Chakraborty et al. (2005) for the respective sites. All the spectra were tied to an absolute flux scale using zeropoints determined from *UBVRI* mag-

nitudes. To tie the spectra with photometry, individual spectrum is multiplied by wavelength dependent polynomial function and it's *BVRI* filter-response convolved fluxes are compared with photometric fluxes at corresponding epoch. The multiplied polynomial is tuned to minimize the flux difference and obtain the tied spectrum. The one-dimensional spectra are corrected for heliocentric velocity of the host galaxy ( $778 \text{ km s}^{-1}$ ;§1) using *dopcor* tasks.

## 3 EXTINCTION

In order to derive intrinsic properties of explosion, the reddening due to interstellar matter in both the Milky Way and the host galaxy, towards the sight-line of SN 2012aw should be known accurately. Using all-sky dust-extinction map of Schlegel et al. (1998), we derived the value of Galactic reddening as  $E(B - V)_{\text{MW}} = 0.0278 \pm 0.0002$  mag. The reddening due to host galaxy  $E(B - V)_{\text{host}}$  was estimated using two methods viz. the blackbody approximations to the 4d fluxes and the narrow blended NaI doublet absorption lines in the spectra.

The observed spectral energy distribution (SED) of a few days old SNe can be approximated as a blackbody and hence, we generated observed spectral fluxes between  $0.26 \mu\text{m}$  to  $0.81 \mu\text{m}$  using photometric data at 4d in *uvw1* band ( $\lambda_c = 2600 \text{ \AA}$ ) of *Swift* Ultra-violet Optical Telescope (UVOT) taken from Bayless et al. (2013) and in *UBVI* bands from the present study. The 4d data for UVOT filters *uvw2* ( $\lambda_c = 1928 \text{ \AA}$ ) and *uvm2* ( $\lambda_c = 2246 \text{ \AA}$ ) are not used because of higher errors and also we did not rely on *R* flux because of the high contamination due to  $H\alpha$  emission. In Fig. 2, we have plotted the dereddened observed fluxes for varying  $E(B - V)$  and here, the dereddening is done using reddening law of Cardelli et al. (1989) for a total-to-selective extinction ratio ( $R_V$ ) of 3.1. We also show the corresponding blackbody model fluxes with best-fit temperatures; and corresponding to  $E(B - V)$  of 0.028 mag, we derive a temperature of 14.2 kK. For  $E(B - V) = 0.25$  mag, we obtain an unphysical high temperature of 32 kK. The theoretical modelling of Dessart & Hillier (2006); Bersten et al. (2011) indicate that a value of temperature above 20kK is not expected for 4d old type IIP SNe and hence we derive an upper limit for total  $E(B - V)$  of 0.15 mag.

The equivalent width (EW) of NaID absorption feature is found to be correlated with the reddening  $E(B - V)$  estimated from the tail of SN Ia color curves (Barbon et al. 1990; Turatto et al. 2003), though it may be a bad proxy in certain cases, e.g. see Poznanski et al. (2011). In the low-resolution spectra presented in this work, it is not possible to resolve the individual component of NaI doublet ( $D_1$   $5889.95\text{\AA}$  and  $D_2$   $5895.92\text{\AA}$ ) and hence we can expect to see the blended feature at the gf-weighted rest wavelength of  $5893\text{\AA}$ . At all the 14 phases of spectra, a weak impression of NaID due to the host is seen overlaid on the broad P Cygni profile due to SN (see Fig. 3), whereas, the feature due to Milky Way is comparatively weak and it is visible only for spectra with high SNR. In Table 5, we list the EW of NaID due to host galaxy only and no attempt is made to estimate EW due to Milky Way. Due to poor SNR ( $< 50$ ; Table 4), the 16d, 104d and 270d spectra were not included in the EW determination. The error in EW is cal-

**Table 4.** Journal of optical spectroscopic observations of SN 2012aw. The spectral observations are made at 14 phases between 7d to 270d.

UT Date (yy/mm/dd.dd)	JD 2456000+	Phase <sup>a</sup> (days)	Range <sup>b</sup> $\mu\text{m}$	Telescope <sup>c</sup>	Grating (gr mm <sup>-1</sup> )	Slit width ( $''$ )	Dispersion ( $\text{\AA}$ pix <sup>-1</sup> )	Exposure (s)	S/N <sup>d</sup> (pix <sup>-1</sup> )
2012-03-22.752	9.25	7	0.38–0.68	HCT	600	1.92	1.43	900	85
			0.58–0.84	HCT	600	1.92	1.26	900	66
2012-03-23.768	10.26	8	0.33–0.63	IGO	300	1.50	2.75	900	147
2012-03-27.615	14.12	12	0.38–0.68	HCT	600	1.92	1.49	1200	123
			0.58–0.84	HCT	600	1.92	1.26	900	75
2012-03-30.659	17.16	15	0.38–0.68	HCT	600	1.92	1.49	900	91
			0.58–0.84	HCT	600	1.92	1.26	900	68
2012-03-31.809	18.30	16	0.38–0.68	HCT	600	1.92	1.49	900	48
			0.58–0.84	HCT	600	1.92	1.26	900	35
2012-04-04.714	22.21	20	0.38–0.68	HCT	600	1.92	1.61	1200	127
			0.58–0.84	HCT	600	1.92	1.25	1200	86
2012-04-10.715	28.21	26	0.38–0.68	IGO	600	1.50	1.39	2700	112
			0.58–0.83	IGO	600	1.50	1.16	1200,2104	71
2012-04-15.802	33.30	31	0.33–0.63	IGO	300	1.50	2.89	1800x2	171
2012-04-29.685	47.18	45	0.33–0.63	IGO	300	1.50	2.89	1200x2	114
2012-05-09.713	57.22	55	0.38–0.68	HCT	600	1.92	1.61	1200	139
			0.58–0.84	HCT	600	1.92	1.25	1200	104
2012-05-15.680	63.19	61	0.38–0.68	IGO	600	1.50	1.38	1800	103
			0.58–0.83	IGO	600	1.50	1.16	1800	85
2012-05-20.730	68.23	66	0.38–0.68	HCT	600	1.92	1.61	900	95
			0.58–0.84	HCT	600	1.92	1.25	900	64
2012-06-27.629	106.13	104	0.38–0.68	HCT	600	1.92	1.61	1200	56
			0.58–0.84	HCT	600	1.92	1.25	1200	38
2012-12-10.846	272.37	270	0.38–0.68	HCT	600	1.92	1.43	2400	26
			0.58–0.84	HCT	600	1.92	1.26	2400	20

<sup>a</sup> With reference to the burst time JD 2456002.59

<sup>b</sup> For transmission  $\geq 50\%$

<sup>c</sup> HCT : HFOSC on 2 m Himalyan Chandra Telescope, Hanle; IGO : IFOSC on 2 m IUCAA Girawali Observatory, India.

<sup>d</sup> At 0.6  $\mu\text{m}$

culated using the relation given by Vollmann & Eversberg (2006) for weak-line limit. The weighted mean of EW derived from 11 individual measurements is  $0.394 \pm 0.067 \text{\AA}$ . Employing empirical relation from Poznanski et al. (2012b), i.e.  $\log_{10} E(B - V)_{\text{host}} = 1.17 \times \text{EW} - 1.85 \pm 0.08$  (where EW in  $\text{\AA}$ ), a value of  $0.041 \pm 0.011$  mag is obtained for reddening due to host galaxy and the error quoted here includes both that in EW and that in the empirical relation. This value is consistent with the  $E(B - V)_{\text{host}} = 0.055 \pm 0.014$  mag which is derived by Van Dyk et al. (2012) using high-resolution Echelle spectra of SN 2012aw obtained from 10-m Keck telescope at 25d. We derive a weighted mean of the two above measurements, i.e.  $0.046 \pm 0.008$  mag for the host galaxy and by adding the Galactic reddening, a total  $E(B - V)_{\text{tot}} = 0.074 \pm 0.008$  mag is derived for SN 2012aw and is adopted throughout this paper. This corresponds to a visual extinction  $A_V = 0.23 \pm 0.03$  mag, assuming line-of-sight ratio of total-to-selective extinction  $R_V = 3.1$ .

## 4 OPTICAL LIGHT-CURVE

### 4.1 Apparent magnitude light-curves

The optical light-curve of SN 2012aw in *UBVRI* filters is shown in Fig. 4. The photometric measurements are made at 54 phases during 4d to 269d. The SDSS *griz* magnitudes are converted to *BVRI* using empirical relations

**Table 5.** Equivalent widths of Na1D absorption feature due to host galaxy.

UT Date (yyyy-mm-dd)	Phase <sup>a</sup> (day)	EW $\text{\AA}$
2012-03-22	7	0.415 $\pm$ 0.204
2012-03-23	8	0.410 $\pm$ 0.185
2012-03-27	12	0.400 $\pm$ 0.233
2012-03-30	15	0.374 $\pm$ 0.361
2012-04-04	20	0.399 $\pm$ 0.172
2012-04-10	26	0.370 $\pm$ 0.226
2012-04-15	31	0.364 $\pm$ 0.189
2012-04-29	45	0.413 $\pm$ 0.276
2012-05-09	55	0.363 $\pm$ 0.237
2012-05-15	61	0.419 $\pm$ 0.233
2012-05-20	66	0.400 $\pm$ 0.272
Weighted mean		0.394 $\pm$ 0.067

<sup>a</sup> With reference to the time of explosion JD 24546002.59

given by Jordi et al. (2006) and are over-plotted. For comparison the light-curves of archetypal type IIP SN 1999em (Leonard et al. 2002a) is also shown. The early light-curve shows sharp initial rise of brightness in all the optical bands and then declining slowly into plateau-phase followed by a sharp fall at around 110d to the nebular-phase. On the con-

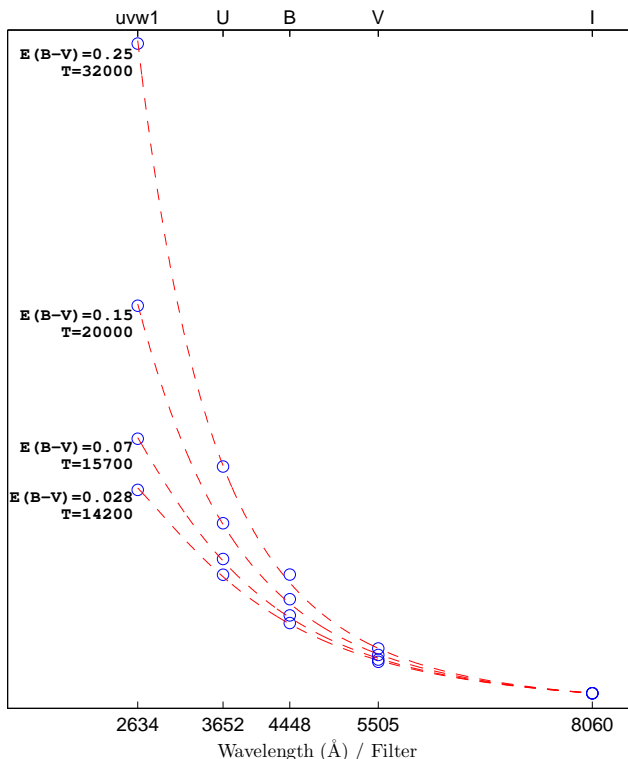


**Figure 2.** The spectral energy distribution of SN 2012aw at 4d is compared with blackbody function. The open circles denote observed fluxes in *uvw1*, *U*, *B*, *V* and *I* bands corrected for respective reddening values while the dotted line is the best-fit models for different temperature. The fluxes are normalized relative to I-band flux.

trary, the observations in UVOT bands do not show any initial rise in the light-curve observed since as early as 3d (Bayless et al. 2013). The peak in early-time light-curve occurs at about 8d, 11d, 15d, 22d, 24d respectively for *UBVRI* bands, followed by a continuous decline in *UB* and a short decline then a continuous rise in *VRI* peaking at 52d, 56d and 71d respectively (see inset in Fig. 4). The early-time light-curve of SN 2012aw is almost similar to other nearby ( $\leq 11$  Mpc), well-studied normal type IIP SNe, e.g. in SN 1999em - *UBV* peaked at 6d, 8d and 10d (Leonard et al. 2002a); in SN 2004et, *UBVRI* peaked at 9d, 10d, 16d, 21d and 25d (Sahu et al. 2006); in SN 1999gi, *BV* peaked at 8d and 12d (Leonard et al. 2002b). Appearance of initial peaks in *UBVRI* seems to be a generic feature of early-time light-curves of IIP SNe and in absence of early-time data, it can provide a good handle on estimating the time of explosion with accuracy of a few days, e.g. at *V*-band, the initial peak occurs at  $13 \pm 3$  d for well studied IIP SNe. Unlike other SNe, the densely-sampled light-curve of SN 2012aw offers the opportunity to see, for the first time, the minima near 42d in *V*, 39d in *R*, 31d in *I* band and then a slow rise to a plateau at about 51d, 59d and 73d respectively. The change in flux from initial early-time rise to the minima is about 16% ( $\sim 0.18$  mag) in *V*, 6% ( $\sim 0.07$  mag) in *R*, 2% ( $\sim 0.02$  mag) in *I*. We note that these values are larger than the typical photometric errors at these epochs. This observed minima around which the SN cools down to hydrogen recombination temperature  $\sim 6000$  K, most likely marks the tail-end of the

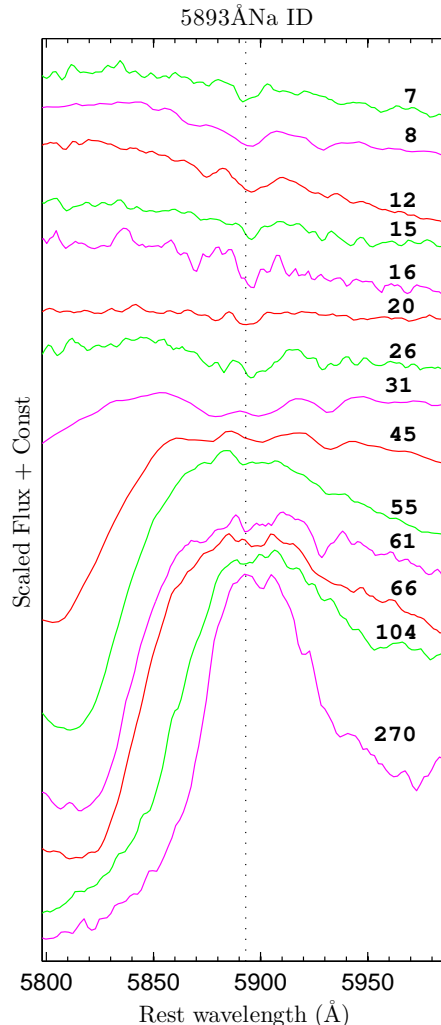


**Figure 3.** The Na I D blended feature due to host galaxy at around 5893Å is shown by dotted line.

flux from the adiabatic cooling phase of the shock-breakout and the dominance of the flux from the hydrogen recombination phase in the supernova envelope (Kasen & Woosley 2009; Cowen et al. 2010; Roy et al. 2011). However, a dense coverage of this early time data for more number of events would be required to confirm the nature and exact cause of this re-brightening in the light-curves.

As the SN goes behind the sun, we have a data gap between 105d to 214d, however, a prolonged plateau phase of about 100d is apparently seen. The decline rates up to 104d after maxima in *UBV* is 5.60, 1.74, 0.55 mag/100d respectively, which is similar to the values observed for SN 1999em (see Fig. 4) and to SN199gi (Leonard et al. 2002b). The rate of decline for SN 2004et is a bit higher, e.g. at *B*-band it is 2.2 mag/100d. During plateau-phase, *R*-band light-curve shows almost no change in brightness, whereas the *I*-band shows slow increase in brightness until mid-plateau of  $\sim 60$  days, then it remains almost constant until the end of plateau. The decline rate (mag/100d) in light-curve of the nebular phase between 215d to 269d is estimated as 1.24, 0.88, 0.88, 0.81, and 0.95 respectively for *UBVRI*.

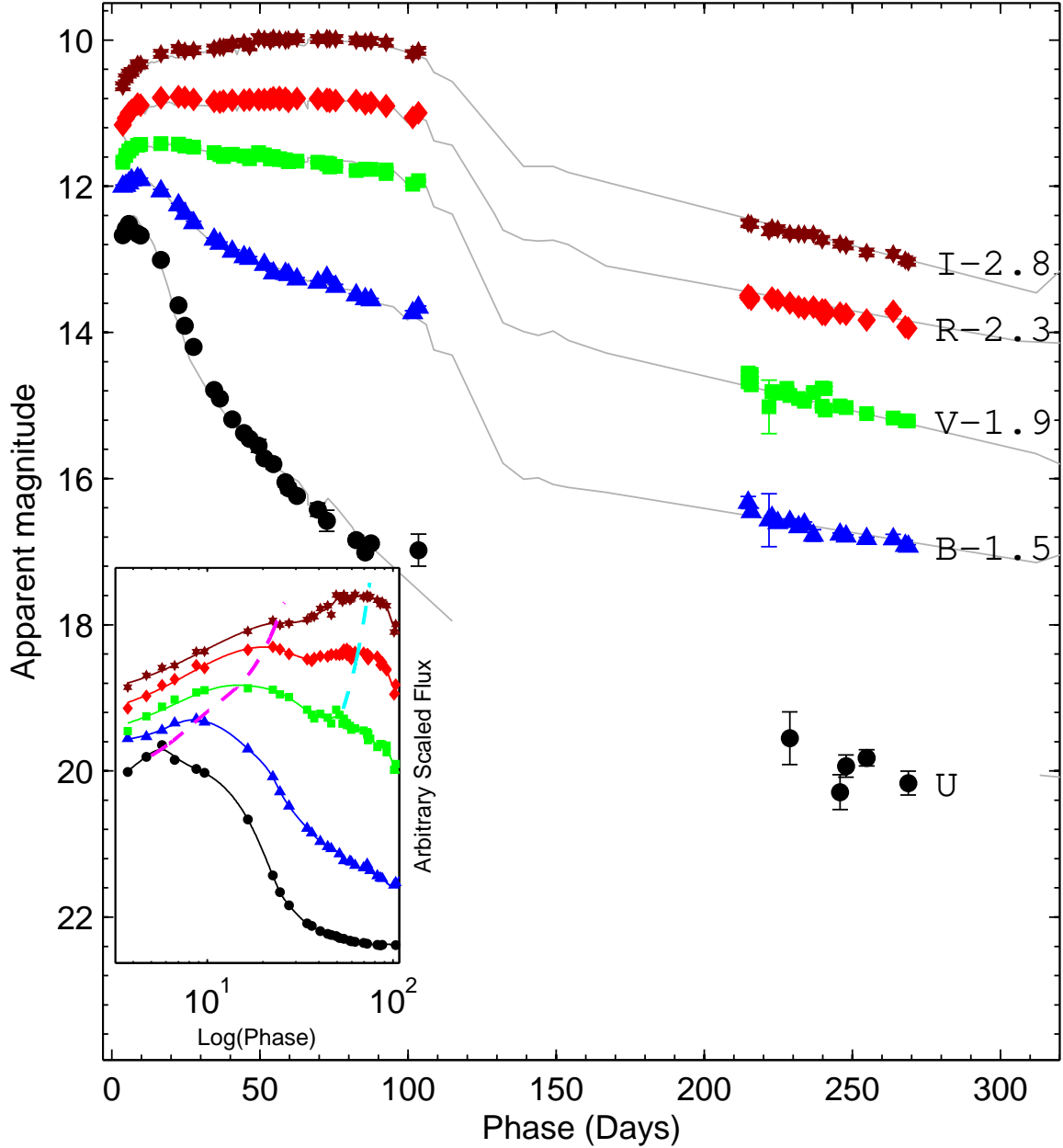


**Figure 4.** The photometric light-curve in Johnson-Cousins *UBVRI* system. The light-curves are shifted for clarity, while for SN 1999em (gray solid lines), it is scaled in magnitude to match with SN 2012aw. The evolution of early-time time light-curve is shown in inset, wherein, the primary peaks in *U*, *B*, *V*, *R*, and *I* at 6d, 9d, 14d, 20d and 23d respectively; and the secondary peak in *V*, *R* and *I* at 52d, 56d, and 71d respectively are clearly visible. Primary and secondary peaks of the light-curve are connected by pair of dashed lines (magenta and cyan respectively).

#### 4.2 Absolute magnitude and color evolution

After correcting for distance and extinction (§3; Table 1), the absolute magnitude *V*-band light-curve is shown in Fig. 5 and it is compared with other well-studied SNe of normal type IIP 1999em, 2004et, 1999gi, 2004dj; subluminous type IIP 2005cs and peculiar type II 1987A. The *V*-band light-curves of SNe from literature are also corrected for distance and extinction and the time of explosion for all (except SN 2004dj) of them is known with an accuracy of a day. The comparison shows striking similarity with SN 1999em in both shape and flux. If we ignore the effect of distance,

then the duration of plateau, the nebular phase luminosity and the overall shape of light-curve are similar for SNe 1999em, 1999gi, and 2012aw; in contrast to that seen for SNe 2005cs and 2004et. For SN 2012aw the plateau-to-nebular phase transition occurs at  $\sim 117$ d and the mid-plateau  $M_V^p$  is  $-16.66$  mag and hence it belongs to a normal type IIP events (Patat et al. 1994), in contrast to the subluminous IIP like 2005cs with  $M_V^p \sim -15$  mag (Pastorello et al. 2009). The peak absolute magnitude of SN 2012aw is equal to that of SN 1999em, about 0.31 mag brighter than SN 1999gi and about 0.49 mag fainter than SN 2004et. The light-curve



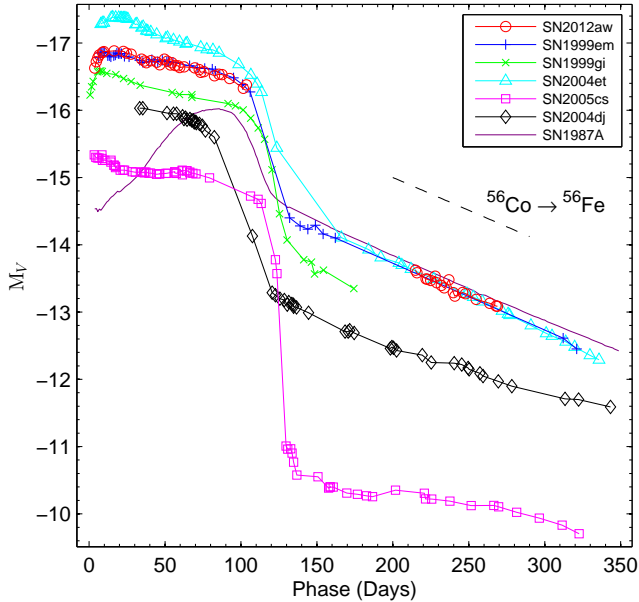


**Figure 5.** Comparison of  $M_V$  light curve of SN 2012aw with other type IIP SNe. The exponential decline of the radioactive decay law is shown with dashed lines. The time of explosion in JD-2400000, distance in Mpc, reddening  $E(B - V)$  in mag and the reference for apparent V-band magnitude, respectively, are : SN 1999em – 51475.6, 11.7, 0.10; Leonard et al. (2002a); Elmhamdi et al. (2003); SN 2004et – 53270.5, 5.4, 0.41; Sahu et al. (2006); SN 2005cs – 53549.0, 7.8, 0.11; Pastorello et al. (2009); SN 2004dj – 53187.0, 3.5, 0.07; Tsvetkov et al. (2008); SN 1987A – 46849.8, 0.05, 0.16; Hamuy & Suntzeff (1990); SN 1999gi – 51522.3, 13.0, 0.21; Leonard et al. (2002b).

evolution in the nebular phase follows the decay rate 0.92 mag/100d. The photometric evolution of type IIP SNe in nebular phase is powered by the radioactive decay of  $^{56}\text{Co}$  into  $^{56}\text{Fe}$  and the expected decay rate is  $(100\text{d})^{-1}$ . The values for SN 2012aw is consistent with this.

The evolution of broad-band colors provides important clues for the expansion and cooling behavior of the supernova envelope. In Fig. 6, the evolution of intrinsic colors  $U - B$ ,  $B - V$ ,  $V - R$  and  $V - I$  are shown. The  $U - B$  color evolves very rapidly in early phases up to  $\sim 50\text{d}$ , primarily due to high temperature and rapid cooling; and it becomes redder from  $-0.94$  to  $1.11$  mag; though it evolves slowly thereafter and reaches  $1.96$  mag by  $90\text{d}$ . By  $260\text{d}$ , it becomes blue again by  $0.6$  mag in about  $150\text{d}$ . The  $B - V$  also evolves similar to  $U - B$ , and in nebular phases both colors follow the evolution completely similar to SN 1987A. The evolution in all the colors shows striking resemblance to that of SN 1999em. The  $V - I$ ,  $V - R$  and  $B - V$  colors of SN 2012aw are significantly ( $\sim 0.2$ - $0.8$  mag) bluer than that of SN 2004et at all phases, while the  $U - B$  color is observed to be redder.

In order to have an idea on the temporal evolution of temperature, we fitted blackbody on the observed fluxes in  $uvw1$  band (data taken from Bayless et al. 2013) and in  $UBVRI$  bands covering the wavelength region  $0.26$ - $0.81 \mu\text{m}$ . The  $uvm2$  and  $uvw2$  bands are not used as these have large uncertainties in magnitudes and also they result in unrealistic blackbody fits at early phases. The fluxes were cor-

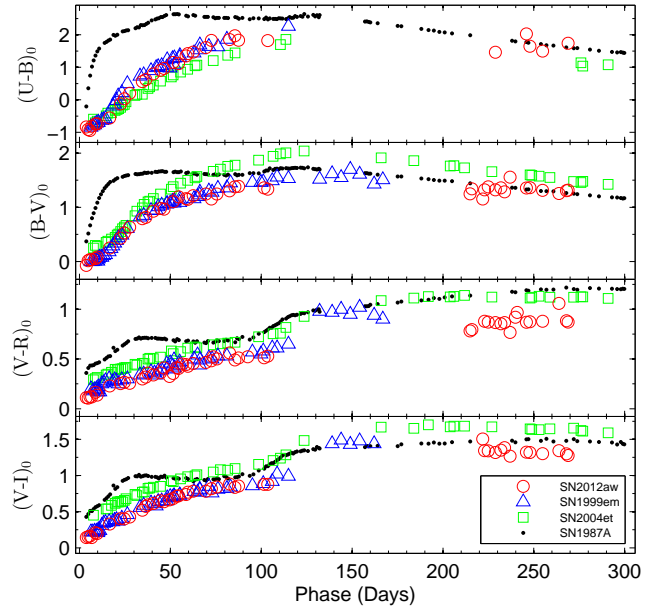


**Figure 6.** The evolution of intrinsic colors of SN 2012aw is compared with other well-studied normal type IIP SNe 1999em, 1999gi and 2004et. The reference for the data is same as in Fig. 5.

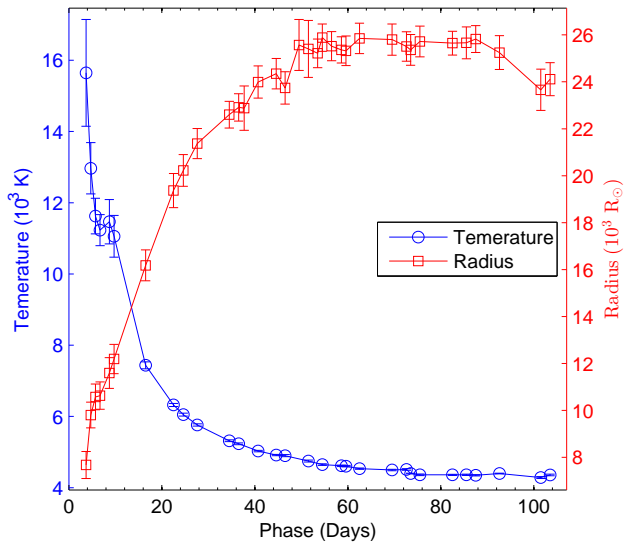


**Figure 7.** The temperature and radius of SN 2012aw as derived from blackbody fits to the observed fluxes in the ultraviolet-optical range  $0.17$ - $0.88 \mu\text{m}$ .

rected for interstellar extinction and we also applied dilution factors as per the prescription by Dessart & Hillier (2006). The fitted values of temperature and the radius are plotted in Fig. 7. The blackbody temperature ( $T_{\text{bb}}$ ) thus derived can be approximated as a photospheric temperature. During the phases 4-10d, the ejecta temperature drops from  $16$  kK to  $11$  kK and by  $20\text{d}$  it drops down to about  $6500$  K, with a very slow decline thereafter to  $4300$  K by  $104\text{d}$ . This indicates that the plateau seen in the absolute magnitude light-curve between  $\sim 20\text{d}$  to  $104\text{d}$  is mainly sustained by the recombination of hydrogen. The sharp change in slope of

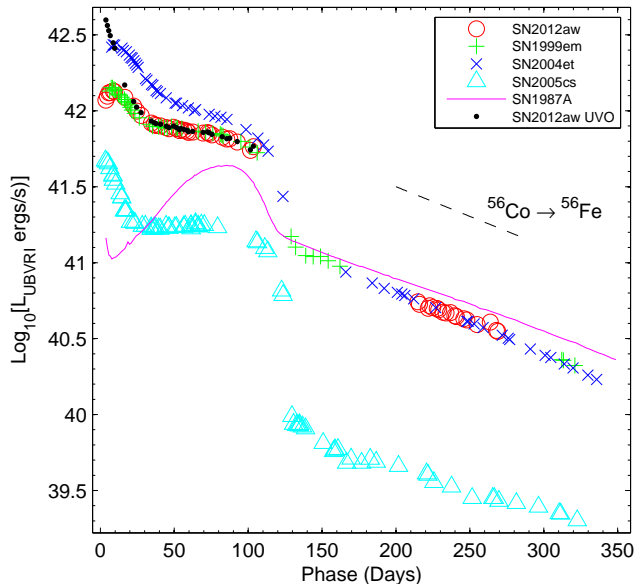


**Figure 8.** The *UBVRI* bolometric light-curve of SN 2012aw is compared with other well studied supernovae. The adopted distances, reddening and time of explosion are same as in Fig. 5. The exponential decline of the radioactive decay law is shown with dashed lines.

$T_{bb}$  around 20-30d is consistent with the similar trend seen in the color-curve evolution of  $U - B$  and  $B - V$ .

### 4.3 Bolometric light-curve

The bolometric light-curves provide constraint on the amount of radioactive  $^{56}\text{Ni}$  synthesized during explosion as well as on the energy of supernova explosion. At early phases ( $\leq 30\text{d}$ ), when supernova ejecta is hotter, the major contribution ( $\sim 80\%$ ) to the bolometric light comes from the ultraviolet and *UB* bands, while at later phases the flux contribution from *RI* and near-infrared band dominates (Misra et al. 2007). Here, we determine pseudo-bolometric light-curve by integrating a spline fitted on the *UBVRI* fluxes derived at their respective effective wavelengths using zero-points from Fukugita et al. (1995). Fluxes are integrated over wavelength range from  $3335 \text{ \AA}$  to  $8750 \text{ \AA}$ ; the lower and upper bounds are extended to the HWHM (half width half maximum) of *U* and *I* bands. Wherever, the observations in a bandpass were missing, the magnitudes were obtained by interpolating the light-curves using low-order cubic-spline. In order to remove the effect of overlapping wavelengths in the *UBVRI* passbands on the determination of SED from observed fluxes, we equated the known splines convolved with the filter response with that of the observed fluxes. As a guess, we provide initial SED as the spline fitted on observed fluxes and iteratively we construct the true spline SED (whose filter-convolved fluxes matches with observed fluxes). In Fig. 8, we plot the bolometric light-curve of SN 2012aw and in the same figure we also show the bolometric light derived using UVOT fluxes in *uvw2* and *uvw1* bands taken from Bayless et al. (2013). The *uvw2* flux is not used due to less number of measurements and large uncertainties in magnitudes. To en-

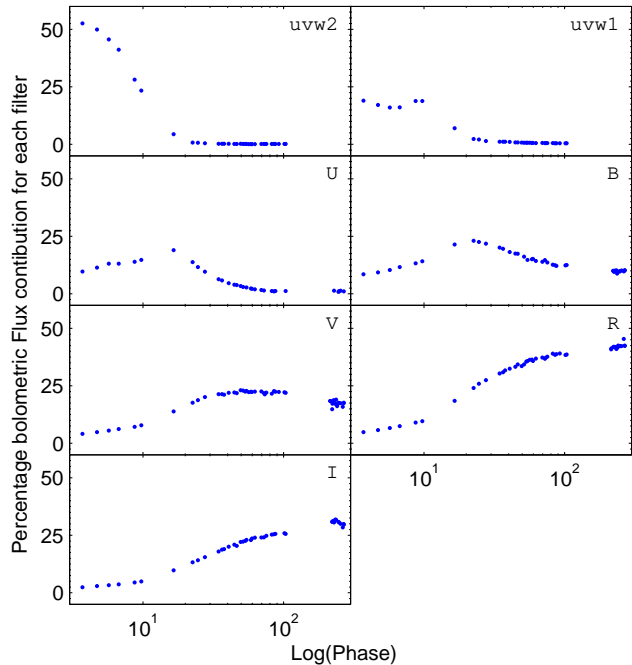


**Figure 9.** The percentage flux contribution in different passbands in the UVOT *uvw2*, *uvw1* and optical *UBVRI*. Fluxes are corrected for extinction.

sure proper comparison, we have applied same scheme to compute bolometric light-curve in *UBVRI* bands for other well-studied type II SNe 1987A (Hamuy & Suntzeff 1990), 1999em (Leonard et al. 2002a), 2004et (Sahu et al. 2006) and 2005cs (Pastorello et al. 2009). Similar to color-curve, the evolution of bolometric luminosity is also similar to SN 1999em. The bolometric luminosity declines rapidly by 0.5 dex in first 30d of evolution, and then it slowly declines by 0.2 dex by 104d.

In Fig. 9, we plot the percentage flux contribution in reference to the total bolometric light in the ultraviolet-optical region ( $0.17$  to  $0.88 \mu\text{m}$ ) from the different passbands. The contribution due to UVOT bands and the optical *UB*, show a sudden change at around 20d. In *uvw2*, the contribution falls from approximately 50% to 0%; in *uvw1*, it drops to 0% from a level of 25%; while in *U* and *B*, it rises from 10% at 4d to 22% at about 20d and falls slowly thereafter to a few percent level in plateau and nebular phases. In *V*, *R* and *I* bands, the trend in flux contribution behaves in a similar fashion and it slowly rises from a few % at 7d to above 25% in the plateau phases and beyond. The bolometric luminosity at 25d and beyond is mainly contributed by the *VRI* bands.

### 4.4 Mass of nickel

In type IIP SNe, the radioactive  $^{56}\text{Ni}$  is synthesized by explosive burning of Si and O during shock breakout phase of the explosion (Arnett 1980) and hence the nebular phase light-curve is mainly powered by radioactive decay of  $^{56}\text{Ni}$  to  $^{56}\text{Co}$  with half-life time of 6.1d and  $^{56}\text{Co}$  to  $^{56}\text{Fe}$  with  $e$ -folding time of 111.26d emitting energetic  $\gamma$ -rays and positrons. The nebular phase luminosity is assumed to be directly propor-

tional to mass of  $^{56}\text{Ni}$ . For a nearby type II-pec SN 1987A, the mass of  $^{56}\text{Ni}$  ( $M_{\text{Ni}}$ ) has been determined fairly accurate to be  $0.075 \pm 0.005 M_{\odot}$  (Arnett 1996), and hence by assuming similar  $\gamma$ -ray energy deposition and by comparing the bolometric luminosity of SN 1987A at comparable epochs, we can estimate  $M_{\text{Ni}}$  of SN 2012aw. We note that for comparison, we use *UBVRI* bolometric luminosity of 1987A computed in this work (§4.3) instead of already available accurately calculated UV-optical-IR luminosity. For SN 2012aw, the *UBVRI* bolometric luminosity at 240d is estimated using a linear fit over 18 epochs between 210d to 270d, which is  $4.53 \pm 0.11 \times 10^{40} \text{ erg s}^{-1}$ . Similarly for 1987A, it is estimated to be  $5.82 \pm 0.06 \times 10^{40} \text{ erg s}^{-1}$ . The ratio of SN 2012aw to 1987A is found to be  $0.778 \pm 0.021$  and hence we calculate the value of  $M_{\text{Ni}}$  for SN 2012aw to be  $0.058 \pm 0.002 M_{\odot}$ <sup>3</sup>

The value of  $M_{\text{Ni}}$  can be independently estimated using the tail luminosity ( $L_t$ ) as described by Hamuy (2003), assuming the  $\gamma$ -rays emitted during radioactive decay of  $^{56}\text{Co}$  makes the ejecta thermalized viz.

$$M_{\text{Ni}} = 7.866 \times 10^{-44} \times L_t \exp \left[ \frac{(t_t - t_0)/(1+z) - 6.1}{111.26} \right] M_{\odot}$$

where  $t_0$  is the explosion time, 6.1d is the half-life of  $^{56}\text{Ni}$  and 111.26d is the e-folding time of the  $^{56}\text{Co}$  decay emitting energy in the form of  $\gamma$ -rays. We compute  $L_t$  at 11 epochs between 215 to 265 days using the observed *V* magnitude, a bolometric correction of  $0.26 \pm 0.06 \text{ mag}$  during nebular phase (Hamuy 2003), and the adopted reddening and distance (see Table 1). The weighted mean of  $L_t$  is  $8.97 \pm 0.19 \times 10^{40} \text{ erg s}^{-1}$  corresponding to mean phase of 240.35d, and this results in a value of  $M_{\text{Ni}} = 0.057 \pm 0.012 M_{\odot}$ . Taking weighted average of the values derived above using two photometric methods, we adopt value of  $M_{\text{Ni}}$  as  $0.058 \pm 0.002 M_{\odot}$  for SN 2012aw.

We note that the value of  $M_{\text{Ni}}$  estimated for type IIP SNe using bolometric luminosity of nebular phase depends considerably on the adopted distance and extinction. For example, the value of  $M_{\text{Ni}}$  reported in the literature (Takáts & Vinkó 2012, see their Table 1, hereafter TV12) for SNe 2005cs, 1999em and 2004et varies from 0.003 to  $0.008 M_{\odot}$ , from 0.022 to  $0.036 M_{\odot}$ , and from 0.056 to  $0.068 M_{\odot}$  respectively. However, in view of the empirical correlation found between mass of  $^{56}\text{Ni}$  and mid-plateau photospheric velocity by Hamuy (2003) using a large sample of type IIP SNe, the observed object-to-object variation in mass of  $^{56}\text{Ni}$  for the above three cases appears to be realistic as the mid-plateau ( $\sim 50\text{d}$  post explosion) photospheric velocity of SNe 2005cs, 1999em and 2004et estimated using SYNOW modelling of spectra is found to be  $1200 \text{ km s}^{-1}$ ,  $3400 \text{ km s}^{-1}$  and  $3750 \text{ km s}^{-1}$  respectively (TV12). Considering the uncertainty in the adopted distance and extinction for SN 2012aw we anticipate that it produced the amount of  $^{56}\text{Ni}$  equal to or a bit less than that for SN 2004et and this is further corroborated by the fact that the mid-plateau photospheric velocity of SN 2012aw is found to be higher than

that of SN 1999em but similar to SN 2004et at comparable epochs (§5.4).

## 5 OPTICAL SPECTRA

### 5.1 Key spectral features

The spectroscopic evolution of SN 2012aw is presented in Fig. 10, in which a preliminary identifications of spectral features is done as per the previously published lines for type IIP events by Leonard et al. (2002a) and the absorption component of some prominent lines are marked. All the spectra are corrected for recession velocity of the host galaxy (§2.2). The early phase (7d and 8d) spectra can be distinguished with featureless blue continuum having broad P-Cygni profiles of hydrogen H I ( $\text{H}\alpha$  6562.85Å,  $\text{H}\beta$  4861.36Å,  $\text{H}\gamma$  4340.49Å,  $\text{H}\delta$  4101.77Å) and helium He I 5876Å. The He I line disappears by  $\sim 16\text{d}$  as the continuum becomes redder with time corresponding to a sudden drop in  $T_{\text{bb}}$  by a factor of two to 7 kK since early phase. The appearance of He I line since early phases and its disappearance exactly at  $\sim 16\text{d}$  is also seen in SN 1999em (Leonard et al. 2002a). The Balmer lines of H I are seen at all the phases until 270d. The FWHM of the emission component of  $\text{H}\alpha$  decreases from  $\sim 17000 \text{ km s}^{-1}$  at 7d to about  $2500 \text{ km s}^{-1}$  at 270d, indicating a decrease in temperature and opacity of the H I line-emitting regions.

In addition to the regular features of H I and He I, the early (7d and 8d) spectra have a couple of peculiar absorption features. Two weak absorption features are present at  $\sim 4300\text{Å}$  and  $\sim 4850\text{Å}$  while two relatively strong absorption features are seen near  $\sim 5500\text{Å}$  (marked with A) and near  $4500\text{Å}$  (marked with B). Similar features have also been identified in the early spectrum of type IIP SNe 1999em (Leonard et al. 2002a), 1999gi (Leonard et al. 2002b), and 2007od (Inserra et al. 2011). The origin of these features is not completely understood and in most of the cases they are explained as high-velocity component of H I and He I lines, however, the presence of N II lines 4623Å 5029Å and 5679Å have also been explored and these lines cannot be completely ruled out (Baron et al. 2000; Inserra et al. 2012a).

In SN 2012aw, the feature A at 7d is at  $\sim 17665 \text{ km s}^{-1}$  with reference to He I rest wavelength, thus making it  $\sim 7198 \text{ km s}^{-1}$  higher over the existing He I absorption feature velocity. This component decreases to  $\sim 16643 \text{ km s}^{-1}$  at 8d making an offset by  $\sim 6586 \text{ km s}^{-1}$  higher than existing He I feature. Another absorption feature B is also located at a velocity position of  $\sim 21785 \text{ km s}^{-1}$  on 7d in reference to rest  $\text{H}\beta$  making it higher by  $\sim 11293 \text{ km s}^{-1}$  over the existing  $\text{H}\beta$  absorption trough. This feature decreases to  $\sim 21477 \text{ km s}^{-1}$  on 8d. Both of these features tend to decrease in velocity with time, however, none of these features could be detected on 12d and after. The HV absorption features are not seen in  $\text{H}\alpha$ . In Fig. 11, we compare the early-phase spectra with other SNe and it can be seen that such HV features indicating existence of very high-velocity line-forming material have also been observed for SN 1999gi (Leonard et al. 2002b) and SN 1999em (Baron et al. 2000; Leonard et al. 2002a). In the day 1 spectra of SN 1999gi, the HV component was more dominant and it appeared at  $-30000 \text{ km s}^{-1}$  with no trace of normal absorption components. Inserra et al. (2012a) detect HV absorption to  $\text{H}\beta$  and

<sup>3</sup> Using the same method and adopting the distance and extinction as given in Fig. 5, we estimate  $M_{\text{Ni}}$  for comparison SNe 2005cs, 1999em and 2004et as  $0.004 \pm 0.001 M_{\odot}$ ,  $0.053 \pm 0.001 M_{\odot}$ , and  $0.058 \pm 0.001 M_{\odot}$  respectively.

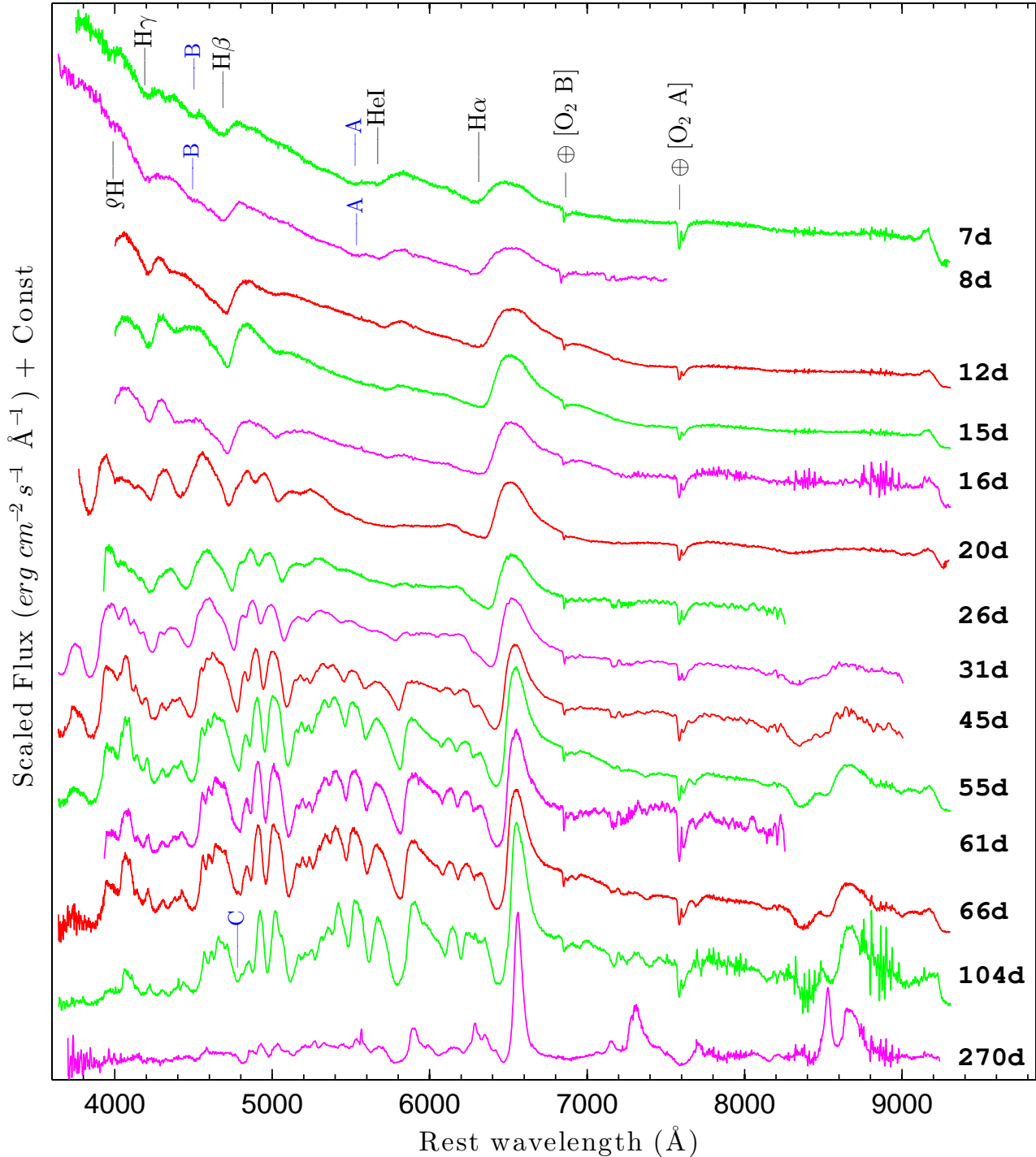


**Figure 10.** The Doppler corrected spectra of SN 2012aw are shown for 14 phases during 7d to 270d. The prominent P-Cygni profiles of hydrogen ( $H\alpha$ ,  $H\beta$ ,  $H\gamma$ ,  $H\delta$ ) and helium ( $He\text{I } 5876\text{\AA}$ ) lines are marked. The peculiar absorption features marked with A, B and C are discussed in text. The telluric absorption features are marked with  $\oplus$  symbol. The portions of spectrum at extreme blue and red end have poor signal-to-noise ratio.

$H\gamma$  lines only in a bright ( $M_v = -18$ ) type IIP SN 2007od, and a detailed spectral analysis using `PHONEIX` favored presence of HV feature. It appears that such high-velocity features in  $H\beta$  and  $He\text{I}$  are ubiquitous in normal luminosity type IIP SNe at early phases ( $\leq 8\text{d}$ ) though its origin (i.e. whether it is caused by abundance and/or density enhance-

ments in the layers of ejecta above photosphere) and exact geometry remains open questions to be addressed using detailed modelling. We attempt to identify these peculiar absorption features using `SYNOW` modelling in §5.2.

The spectra at 12d, 15d and 16d represent transition from a hotter ( $\sim 16\text{kK}$ ) early phase to a cooler ( $\sim 6\text{kK}$ )

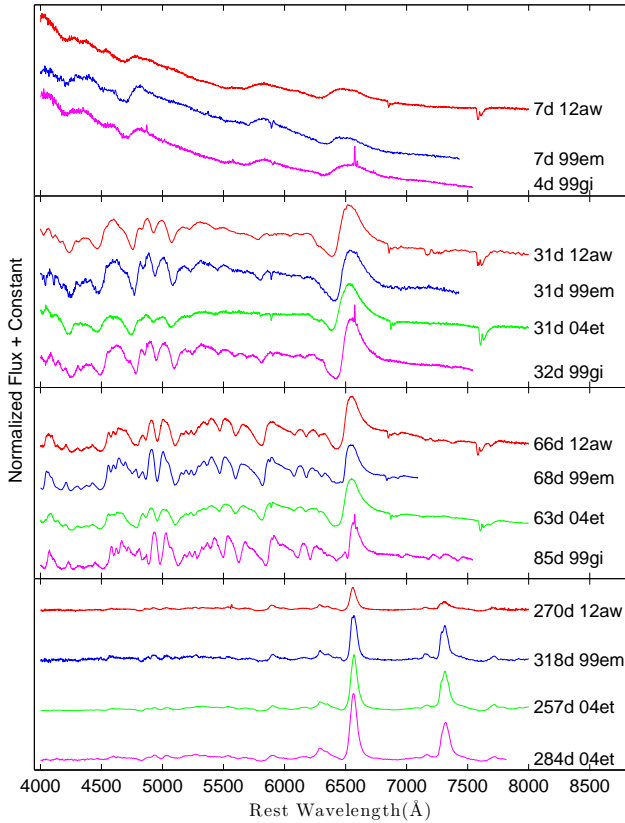


**Figure 11.** Comparison of early (7d), plateau (31d, 66d) and nebular (270d) phase spectra of SN 2012aw with other well-studied type IIP SNe 1999em (Leonard et al. 2002a), 1999gi (Leonard et al. 2002b), 2004et (Sahu et al. 2006; Maguire et al. 2010). Observed fluxes of all the SNe are corrected for extinction and redshift (adopted values same as in Fig. 5).

plateau phase when photosphere begin to penetrate Fe-rich ejecta. These spectra mark the emergence of permitted lines of singly ionized atoms of calcium, iron, scandium, barium, titanium and of neutral sodium atoms. The strong lines of Ba II 4554Å blend and Fe II 5169Å begin to appear at 12d, and the weaker lines of Fe II at 4929Å and 5018Å are clearly seen at 20d. The spectra at 8 epochs from 20d to 104d represent plateau-phase corresponding to further slow cooling of the supernova envelope and appearance of more number of metallic lines. The lines of Na I D 5893Å and Ca II IR Triplet 8498, 8542, 8662Å emerge at 20d and they are clearly visible by 31d. The blend of Ca II H 3934Å & K 3968Å appear at the gf-weighted rest wavelength 3945Å and it is very strong at 20d; seen until 104d. A definite identifications of Ca II is seen in early spectrum of IIP SNe as well, e.g. at 12d in SN 1999em (Baron et al. 2000). The Fe II 5535Å blend, Sc II 5665Å multiplet, Ba II 6142Å, and Sc II 6246Å, are clearly seen at 45d. The above features are present in the spectra until 104d and their comparison with other SNe (Fig. 11) indicate that the plateau phase spectral features are similar to normal type IIP events.

The only late time spectrum at 270d shows emission lines with no absorption components, which is a typical characteristic feature of nebular phase spectra of IIP SNe. A comparison of 270d spectrum are made with other SNe in Fig. 11 and a preliminary identification of nebular lines are

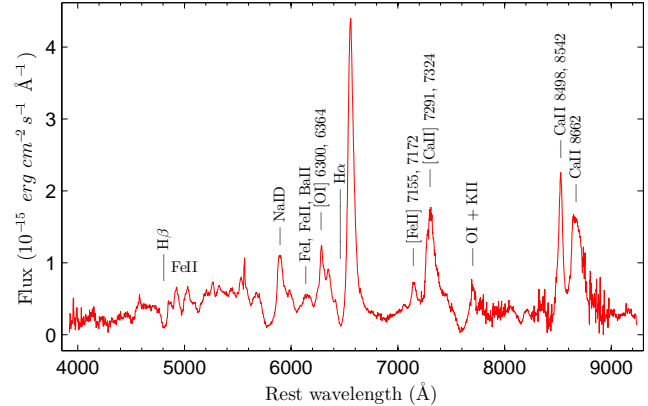


**Figure 12.** The nebular phase spectrum of SN 2012aw at 270d.

shown in Fig. 12. The forbidden emission lines of [O I] 6300, 6364Å, [Ca II] 7291, 7324Å and [Fe II] 7155, 7172 Å; permitted emission lines of H I, Na I 5893Å doublet and Ca II 8600Å triplet become the dominant spectral features.

The presence and evolution of spectral features of SN 2012aw during early, plateau and nebular phases show striking similarity with other well-studied normal type IIP SNe 1999em (Leonard et al. 2002a), 1999gi (Leonard et al. 2002b), and 2004et (Sahu et al. 2006). However, in order to identify and interpret weak spectral features; to estimate the velocities of photospheric/ejecta layers and to understand how the layers of line-forming regions evolve with time and vary among object-to-object, we perform SYNOW modelling of the spectra in the next section.

## 5.2 SYNOW modelling of spectra

We modeled the spectra of SN 2012aw with parameterized supernova spectrum synthesis code `synow 2.34` (Fisher et al. 1997, 1999; Branch et al. 2002). In contrary to the full non-local thermodynamic equilibrium (NLTE) model codes CMFGEN (Dessart & Hillier 2005b) and PHOENIX (Baron et al. 2004), SYNOW assumes - simple LTE model atmospheres having a sharp photosphere emitting a blackbody continuum; a spherically symmetric supernova expanding homologously; the line formation is due to pure resonant scattering and radiative transfer is computed by employing Sobolev approximation. We tried three different options for optical depth profiles (viz., Gaussian, exponential and powerlaw), no significant differences were noticed, however while matching absorption minimum the exponential profile,  $\tau \propto \exp(-v/v_e)$ , were  $v_e$ , a profile fitting parameter, e-folding velocity, was found to be most suitable and is adopted here. One important aspect of SYNOW model is detachment of an ion (line-forming layer) from photosphere which is achieved by setting the minimum velocity of the ion greater than photospheric velocity resulting into flat-topped emission and blue-shifted absorption counterpart. Strong H $\alpha$  P-Cygni can be partially fitted in absorption minima with detached H I only, while the strong emission part remain unfitted with flat-topped crest.

<sup>4</sup> <http://www.nhn.ou.edu/~parrent/synow.html>

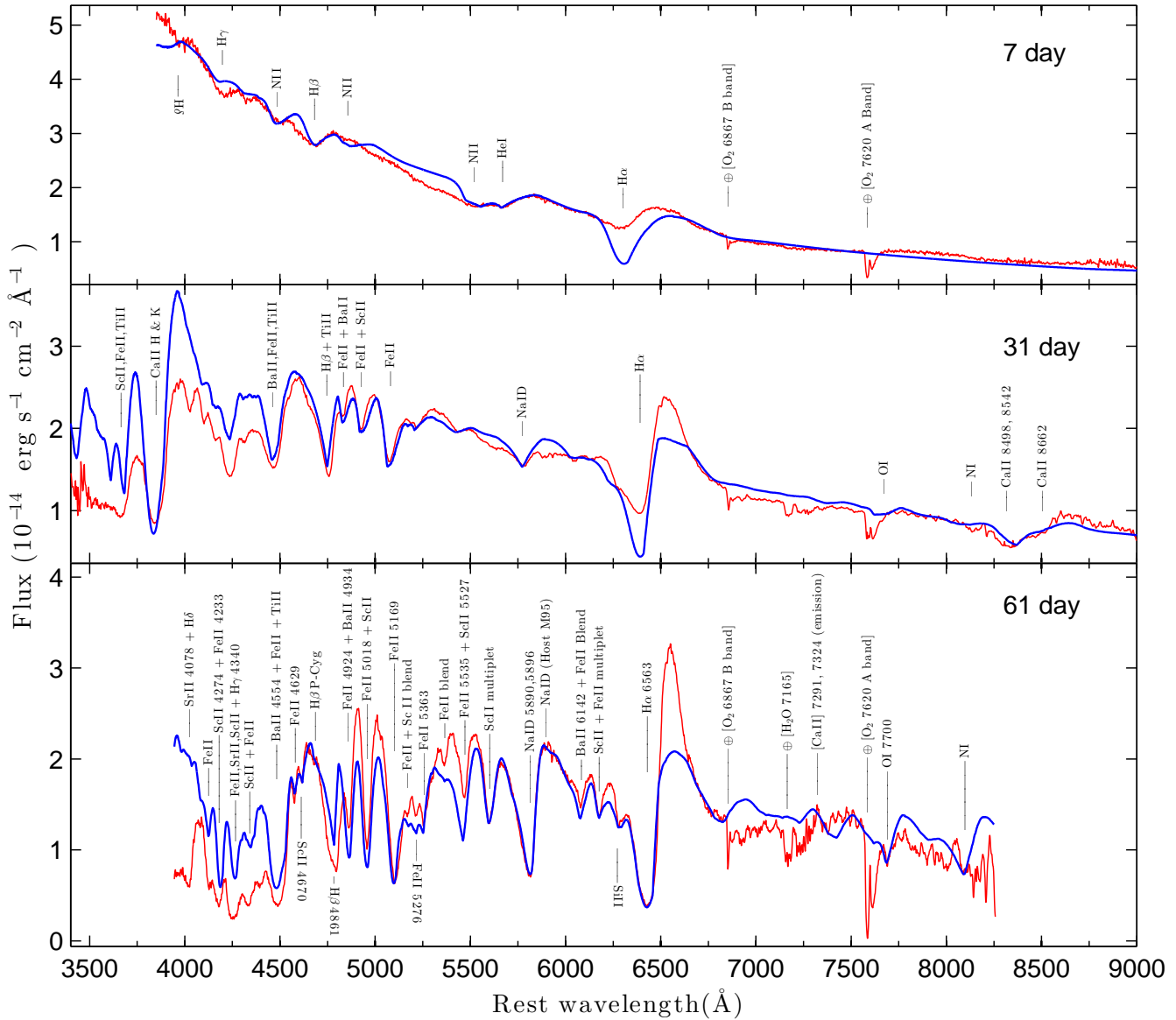


**Figure 13.** SYNOW modelling of 7d, 31d and 61d spectra of SN 2012aw. Model spectra are shown with thick solid line (blue), while the observed ones are in thin solid line (red). Observed fluxes are corrected for extinction.

The observed spectra are Doppler-corrected and dereddened, before visually fitting the model SYNOW spectra with the observed ones. We have modeled the spectra for all the 14 phases and the best-fit values of  $T_{bb}$  to match the continuum are given in Table 6. These SYNOW-derived temperatures are consistent with the ones derived photometrically (§4.2). In the early-phase spectra continuum is fitted properly as it agrees well with the SYNOW’s approximation of LTE atmosphere, whereas at later phases, the continuum is quite deviant, though we are able to match the spectral lines. In Fig. 13, we show the modeled spectra at 7d, 31d and 61d including the common set of contributing species (H I, He I etc) and additional set of species N II; Fe II; Ti II; Sc II; Ca II; Ba II; Na I; Si II; O I and N I respectively. It can be seen that model spectra is able to match and reproduce most of the features present in the observed spectra. The optimization of  $v_{ph}$  is done to match the absorption minima of Fe II mul-

tiplet (4924, 5018, 5169Å) during plateau phase and of He I 5876Å line during early phase spectra.

The 7d spectrum shows well-matched continuum with P-Cygni profiles of H $\alpha$ , H $\beta$ , H $\gamma$ , H $\delta$  and He I. The suspected absorption due to high-velocity component of H $\beta$  and He I are explored further by introducing nitrogen, and the SYNOW modelling appears to be consistent with the absorption dips near 4512Å, 4834Å, 5528Å which correspond to N II lines of rest-wavelength 4623Å, 5029Å and 5679Å respectively. The N II lines of 4623 and 5679Å are also seen in 8d spectrum (Fig. 11) and they disappear thereafter. Using full-LTE modelling with PHONEX of 7d spectrum of SN 1999em, Barbon et al. (1990) have reproduced absorption features using N II lines indicating presence of enhanced nitrogen and helium. We conclude that early-time spectral features of SN 2012aw were very much similar to normal IIP SNe 1999em as well as 1999gi. We however, note that in 5d spectrum



**Table 6.** The best-fit blackbody continuum temperature ( $T_{bb}$ ) and the line velocities of  $H\alpha$ ,  $H\beta$ , Fe II (4924Å, 5018Å, 5169Å) and He I 5876Å as estimated from the SYNOW modeling of the observed spectra of SN 2012aw. Velocities derived using lines of Fe II or He I are taken to represent the velocity of photosphere ( $v_{\text{phm}}$ ).

UT Date (yyyy-mm-dd)	Phase <sup>a</sup> (day)	$T_{bb}^b$ (kK)	$v(\text{He I})$ $10^3 \text{ km s}^{-1}$	$v(\text{Fe II})$ $10^3 \text{ km s}^{-1}$	$v(H\alpha)$ $10^3 \text{ km s}^{-1}$	$v(H\beta)$ $10^3 \text{ km s}^{-1}$
2012-03-22	7	16.5	11.2	-	12.8	11.2
2012-03-23	8	15.5	10.7	-	12.8	11.0
2012-03-27	12	14.0	9.0	-	11.7	9.7
2012-03-30	15	13.5	8.65	-	10.6	9.3
2012-03-31	16	12.5	8.5	8.6	10.4	9.2
2012-04-04	20	10.5	-	7.7	10.0	8.6
2012-04-10	26	7.5	-	6.55	8.8	7.3
2012-04-15	31	7.5	-	5.6	7.9	6.6
2012-04-29	45	5.5	-	4.5	6.4	5.2
2012-05-09	55	5.2	-	4.15	5.5	4.8
2012-05-15	61	5.2	-	3.5	5.0	4.2
2012-05-09	66	5.2	-	3.5	5.0	4.2
2012-06-27	104	4.9	-	2.9	3.8	3.0
2012-12-10	270	3.9	-	1.6	3.4	1.6

<sup>a</sup> With reference to the time of explosion JD 24546002.59

<sup>b</sup> Best-fit blackbody temperature of photosphere to match the continuum in observed spectrum.

of bright type IIP SN 2007od, the presence of absorption dips near 4500Å & 4800Å and absence of dip near 5500Å favored presence of HV components (Inserra et al. 2012a). The He I feature in SN 2012aw disappears at ~16d and a prominent Na I D feature begin to emerge from 26d at similar location. In plateau-phase spectra, we have also incorporated ions Fe II, Sc II, Si II, Ca II and heavy ions Ti II, Ba II of which most are present as blended or weaker features in the spectra.

The lines of Si II at 6347Å and 6371Å appearing as a blend at 6355Å can be seen in the bluer wing of broad P-Cygni  $H\alpha$  absorption, which starts to appear at about 26d when  $T_{bb}$  drops down to about 7500 K and it can be seen until 104d (Fig. 10, 13, & 14). This feature is also seen in the spectra of SN 1999em at similar phases, though it has been identified as a high-velocity component of  $H\alpha$  (Leonard et al. 2002a). In SN 2012aw this feature is fitted well with Si II 6355Å blend in 31d and 61d spectra for the photospheric velocity at respective phases and hence we rule out the possibility of this being a high-velocity component. We note that the Si II feature is also identified in the hotter early time (< 10d) spectra of SN 1999em, which we do not see in SN 2012aw.

The feature marked with C in Fig. 10 is analyzed further using SYNOW modelling. We find that it is most probably a high velocity component of  $H\beta$  blended with Ba II and Ti II lines. A careful inspection of model fits in Fig. 14, it can be seen that this feature actually starts to appear much earlier than 104d. At 55d, a very faint impression of this feature appears which does not fit with the SYNOW model feature of  $H\beta$  and continues to become increasingly stronger until our last plateau spectra at 104d. At 104d (modeled with  $H\beta$  regular and high velocity component blend) this feature became strong enough to suppress the existing regular  $H\beta$  feature and appear as a entire separate absorption component. By SYNOW modelling the 104d spectra, none of the independent atomic species and single  $H\beta$  component

could be accounted for this feature. Only a high velocity  $H\beta$  component of  $\sim 5200 \text{ km s}^{-1}$  along with blend of Ba II and Ti II lines could match the feature, whereas the regular  $H\beta$  component remains in line with the existing velocity trend at a velocity of  $\sim 3000 \text{ km s}^{-1}$  only. Similar problem was also encountered with 104d  $H\alpha$  feature which is not much apparent by eye inspection, but single  $H\alpha$  component in model spectra was unable to fit the broadened  $H\alpha$  absorption dip in the observed spectra. Although no separate absorption dip was seen here, but the absorption feature of  $H\alpha$  is somewhat broadened which only a blend of high velocity component along with regular  $H\alpha$  can fit. This high velocity component is found to be at  $\sim 5800 \text{ km s}^{-1}$  whereas the regular  $H\alpha$  component is at  $\sim 3800 \text{ km s}^{-1}$  which falls in line with the existing  $H\alpha$  velocity evolution. It is also to be noted that velocity difference of high velocity component with the regular component is  $\sim 2000 \text{ km s}^{-1}$  for both  $H\alpha$  and  $H\beta$ , which might indicate that the origin of both high velocity component is from a single H-layer whose velocity is  $\sim 2000 \text{ km s}^{-1}$  higher than the actual layer responsible for photospheric velocity. A careful examination of  $H\beta$  profiles in Fig. 11 at phase 60d indicate that the feature similar to C is absent in the spectra of SNe 1999em and 1999gi, however, this feature is present in spectrum of SN 2004et. The presence of HV components of  $H\alpha$  and  $H\beta$  have been observed through out photospheric phase until 105d in a bright ( $M_V = -17.67$ ) type IIP SN 2009bw (Inserra et al. 2012b) suggestive of interaction between the SN ejecta and the pre-existent circumstellar material (CSM). We, therefore, suggest that the broadening of  $H\beta$  and possibly  $H\alpha$  during 55d to 104d indicate ejecta-CSM interaction in SN 2012aw.

The presence of absorption feature due to O I line at 7774Å is clearly reproduced by SYNOW in the 61d spectrum. The O I line begin to appear at 31d and it is clearly seen until 104d. The N I 8130Å line is marginally detected as its identification is affected by the poor SNR. The absorption

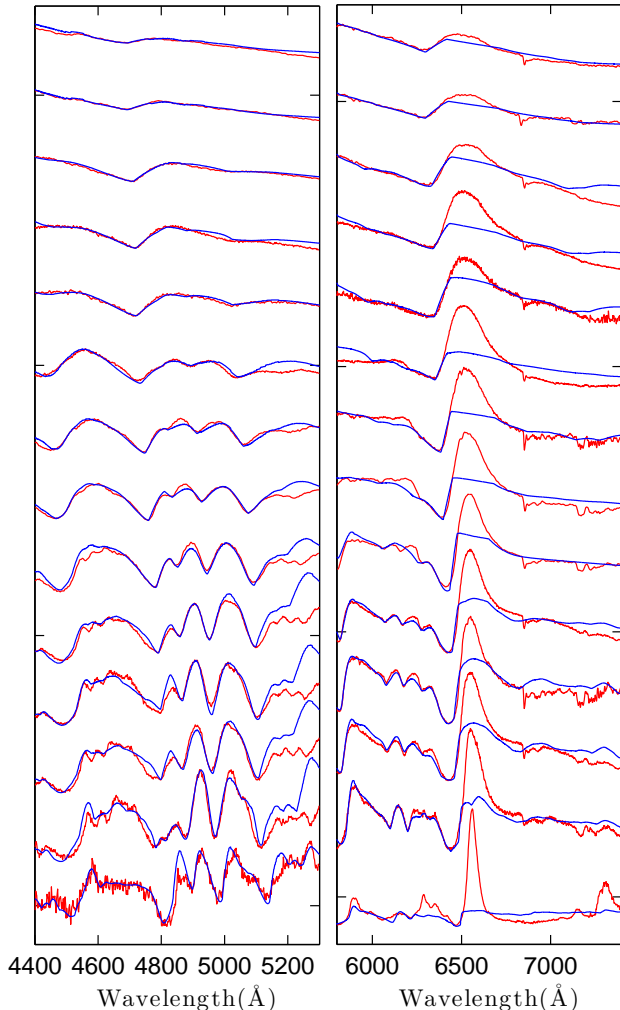


**Figure 14.** SYNOW modelling (blue) for Fe II multiplet (left) and H $\alpha$  (right) profiles over the observed spectra (red) are shown. The spectral evolution is shown top to bottom at 14 phases from 7d to 270d. Detached H is used to fit the absorption dip. In addition to Fe II and H I; other ions (Sc II, Ba II, Si II and Na I, Ti II) are also incorporated in model to fit some weaker features, specially at later phases. The phases of plotted spectra are 7d, 8d, 12d, 15d, 16d, 20d, 26d, 31d, 45d, 55d, 61d, 66d, 104d and 270d (top to bottom).

feature seen  $\sim 9000\text{\AA}$  in 55d and 66d spectra (see Fig. 10) are most likely due to C I 9061 $\text{\AA}$ . The appearance of absorption features in the plateau-phase spectra due to O I and occasionally also due to C I and N I have also been observed in normal type IIP SN 1999em (Leonard et al. 2002a), bright IIP SN 2009bw (Inserra et al. 2012b), subluminous IIP SNe 2009md (Fraser et al. 2011), 2005cs (Pastorello et al. 2009) and 2008in (Roy et al. 2011). Several weak absorption features viz. Fe II 4629 $\text{\AA}$ , Sc II 4670 $\text{\AA}$ , Fe II 5276 $\text{\AA}$  and Fe II 5318 $\text{\AA}$  are identified.

### 5.3 Evolution of spectral lines

The evolution of spectral features provide important clues about the interaction of expanding ejecta with the circumstellar material, formation of dust in the ejecta and geo-

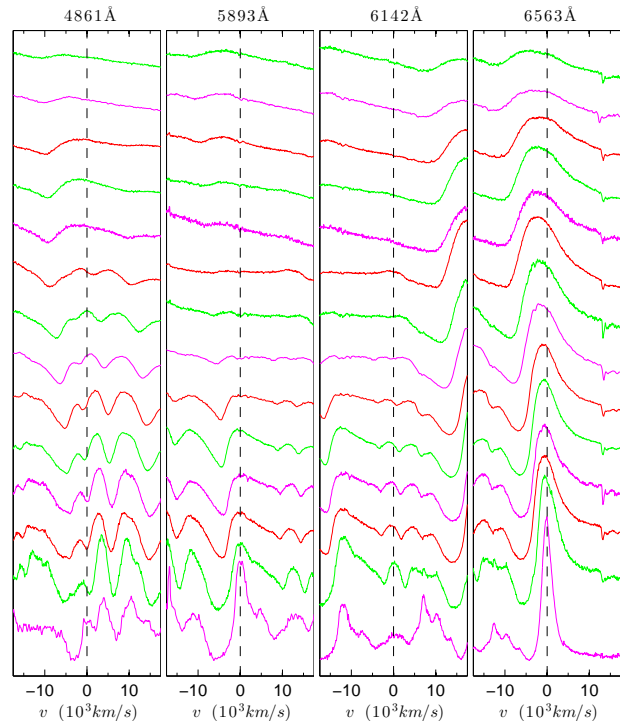


**Figure 15.** Evolution of line profiles for H $\beta$ , Na I D, Ba II and H $\alpha$  are plotted at 14 phases from 7d to 270d top to bottom. The zero-velocity line is plotted with dotted line and the corresponding rest wavelength is written on top. The phases of plotted spectra are 7d, 8d, 12d, 15d, 16d, 20d, 26d, 31d, 45d, 55d, 61d, 66d, 104d and 270d (top to bottom).

metrical distribution of ejecta. To illustrate the evolution of individual lines, a portion of spectrum is plotted in Fig. 15 from 7d to 207d in velocity domain corresponding to rest wavelengths of H $\beta$  4861 $\text{\AA}$ , Na I D 5893 $\text{\AA}$ , Ba II 6142 $\text{\AA}$  and H $\alpha$  6563 $\text{\AA}$ . Broad H $\alpha$  P-Cygni (FWHM  $\sim 17000 \text{ km s}^{-1}$ ) is prominent from as early as first epoch 7d spectra and is present all throughout which evolves into narrow feature (FWHM  $\sim 2500 \text{ km s}^{-1}$  at 270d) with time. Apart from blue-shifted absorption trough of the P-Cygni, which is the indicator of expansion velocity, the emission peak is also blue shifted by  $4500 \text{ km s}^{-1}$  at 7d ( $2700 \text{ km s}^{-1}$  at 15d,  $2100 \text{ km s}^{-1}$  at 31d), it almost disappears by 66d ( $600 \text{ km s}^{-1}$ ) and settles to rest in late plateau spectrum of 104d ( $300 \text{ km s}^{-1}$ ). The blue shift of emission peak in early time (plateau) spectra is also seen in H $\beta$  and such features are similar with that observed in other type II SNe namely SNe 1999em (Elmhamdi et al. 2003), 2004et (Sahu et al. 2006) and 1987A (Hanuschik & Dachs 1987) and it has been theoretically explained as being due to scattering of the photons from the receding part of the ejecta (Chugai 1988; Jeffery & Branch 1990).

A comparison of nebular phase 270d H $\alpha$  line profile with other SNe (Figs. 11, 16) indicate that the H $\alpha$  line flux was lower than that of SNe 1999em and much lower than 2004et. Whereas the FWHM of H $\alpha$  appears to be or similar (i.e.  $\sim 2600 \text{ km s}^{-1}$ ) for these three SNe, suggesting that the expansion velocity of line-emitting region have been quite similar. Moreover, H $\alpha$  appears to be quite symmetric around zero



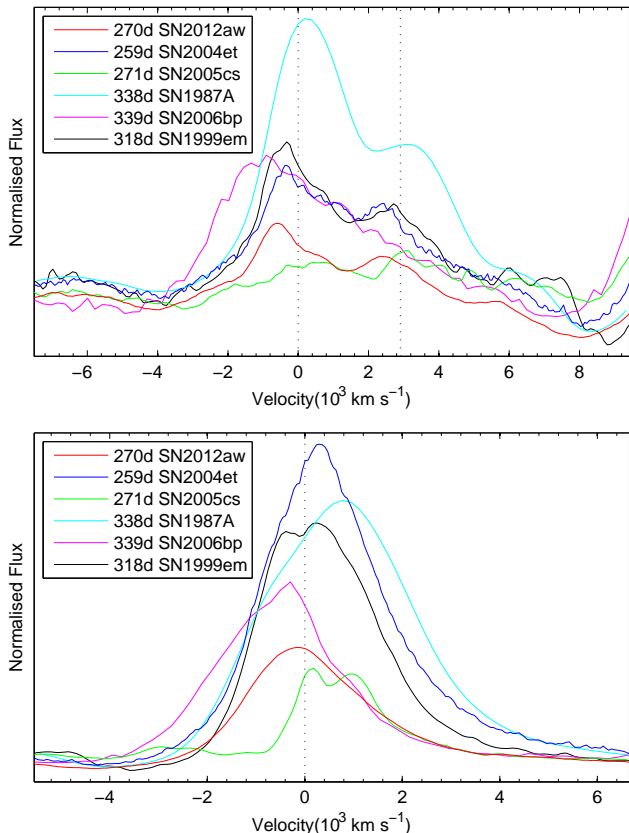


**Figure 16.** The velocity profiles of O I doublet (left) and H $\alpha$  are compared with other SNe from literature. The spectra have been corrected for recession velocities of respective host galaxies. The sources for the spectra are : SN 1987A (Pun et al. 1995), SN 1999em (Leonard et al. 2002a), SN 2004et (Sahu et al. 2006), SN 2005cs (Pastorello et al. 2009), SN 2006bp(Quimby et al. 2007).

velocity indicating a spherically symmetric distribution of hydrogen envelope. This is in contrary to that observed for SN 2006bp, whose profile is highly asymmetric suggesting that explosion have been quite asymmetric or the dust is forming. The blue shift in H $\alpha$  emission peak can also result from preferential attenuation of red wings due to formation of dust in the ejecta. The indication of dust formation is seen in SN 1999em after 500d (Elmhamdi et al. 2003) and in SN 2004et after 320d (Sahu et al. 2006; Maguire et al. 2010). The presence of blueshift ( $\sim 1500 \text{ km s}^{-1}$ ) in H $\alpha$  emission peak have been seen from 226d to 452d spectra of IIP SN 2007od (Inserra et al. 2012b) and this has been explained by presence of dust in the ejecta. We note that observational signatures related to early dust formation and the ejecta-CSM interaction for SN 2012aw are unlike that of bright ( $M_V \sim -18$  mag) IIP SNe 2007od, 2009bw and 2006bp.

The He I 5876 $\text{\AA}$  is prominent from early 7d spectra which disappear rapidly and can be traced only upto 16d. Several metal features start to appear from 26d. The Si II 6355 $\text{\AA}$  feature is found to appear on the blue wing of H $\alpha$  at  $\sim -12000 \text{ km s}^{-1}$  and evolved monotonically until last plateau phase spectra at 104d. The Na I D doublet 5890, 5896 $\text{\AA}$  feature start to appear at position very close to earlier He I feature, and it persists upto nebular phase at 270d. The location of Na I D emission peak at zero velocity indi-

cates an almost spherical distribution of the Na in the ejecta material. The absorption dips due to s-process elements Ba II 6142 $\text{\AA}$  and Sc II 6248 $\text{\AA}$  start to appear and strengthens until the last plateau spectra 104d. The O I lines start to appear at 104d and it is seen clearly in 270d spectrum. Similar to H $\alpha$  line, the O I line flux is too smaller than that of SNe 1999em and 2004et, though the terminal velocity is of similar order (see Fig. 16).

#### 5.4 Ejecta velocity

The expansion velocity of photosphere ( $v_{\text{ph}}$ ) coupled with the mass of ejected matter ( $M_{\text{ej}}$ ) provides strong constraints on the kinetic energy ( $E_{\text{kin}}$ ) of explosion. The photosphere represents the optically thick and mostly ionized part of the ejecta which emits most of the continuum radiation as a “diluted blackbody”. This photosphere is located in a thin spherical shell where electron-scattering optical depth of photons is  $\sim 2/3$  (Dessart & Hillier 2005a). In type IIP SNe, no single measurable spectral feature is directly connected with the true velocity of photosphere, however, during the plateau-phase, it is best represented by blue-shifted absorption components of P-Cygni profiles of Fe II at 4924 $\text{\AA}$ , 5018 $\text{\AA}$  and 5169 $\text{\AA}$ , while in early-phase lines of He I 5876 $\text{\AA}$  or H $\beta$  act as a good proxy (see TV12 for a detailed review on estimating photospheric velocities of type IIP SNe). We can estimate velocities either by measuring Doppler-shift of the absorption minima using SPLIT task of IRAF or by modelling the observed spectra with SYNOW. The later gives better estimate of  $v_{\text{ph}}$  as it can take care and reproduce line blending, however, for the sake of comparing velocities of SN 2012aw with other SNe in literature, we use both the methods in this work and the corresponding velocities are denoted as  $v_{\text{pha}}$  and  $v_{\text{phm}}$  respectively. Apart from Fe II lines, the expansion velocities of line-forming layers for H $\alpha$ , H $\beta$ , He I, and Sc II are also estimated.

Using SYNOW we obtain the best fit locally, for employing the whole wavelength range may lead to over- or underestimate of velocities due to formation of lines at different layers. Fig. 14 shows best fitted profiles over  $\sim 1000\text{\AA}$  wide wavelength regions around H $\alpha$  and Fe II along with H $\beta$  features. It can be seen that the best-fit model spectra are able to reproduce the absorption components of H $\beta$ , Fe II 4924 $\text{\AA}$ , Fe II 5018 $\text{\AA}$ , and Fe II 5169 $\text{\AA}$  simultaneously. At early phases from 7d to 16d, the best-fit model velocity for He I 5876 $\text{\AA}$  line is also estimated. The model-derived velocities are listed in Table 6 and the value of  $v_{\text{phm}}$  represent He I line until 15d and Fe II lines at phases thereafter. The typical uncertainty in velocities estimated by deviation seen visually from best-fit absorption troughs by varying  $v_{\text{phm}}$  is  $\sim 150 \text{ km s}^{-1}$ . This is consistent with the values obtained using automated computational techniques viz.  $\chi^2$ -minimization and cross-correlation methods (TV12).

The expansion line velocities of H $\alpha$ , H $\beta$ , He I, Fe II (4924 $\text{\AA}$ , 5018 $\text{\AA}$  and 5169 $\text{\AA}$ ) components, Sc II 6246 $\text{\AA}$  and Sc II 4670 $\text{\AA}$  blend has also been determined using IRAF by fitting the absorption trough with a Gaussian function and these are shown in Fig. 17. It can be seen that H I (H $\alpha$ , H $\beta$ ) lines formed at larger radii (i.e. higher optical depths) than He I, while the Fe II lines are formed at lower radii. The Sc II lines are formed at even lower optical depths and the velocities derived using Sc II 4670 and 6247 $\text{\AA}$  at phases

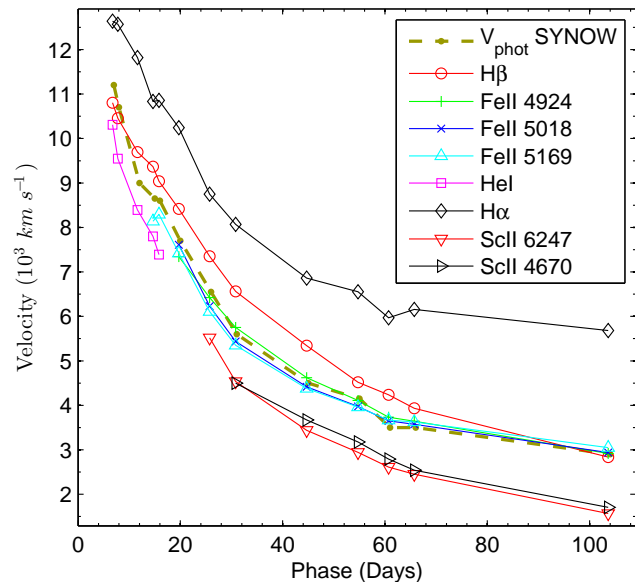


**Figure 17.** Line velocity evolution of  $H\alpha$ ,  $H\beta$ , He I, Sc II and Fe II. The velocities are estimated using Doppler-shift of the absorption minima. The expansion velocity of photosphere ( $v_{\text{phm}}$ ) estimated from SYNOW fits of He I line until 15d and simultaneous fits for Fe II lines at later phases (see Table 6) are overplotted for comparison.

26d onwards are systematically lower by  $\sim 1000 \text{ km s}^{-1}$  from that of Fe II lines or of  $v_{\text{phm}}$ . During 16d to 104d, it can be seen that velocities derived using individual lines of Fe II are same within errors and these values are further in agreement with that determined using SYNOW (i.e. simultaneous fits to Fe II lines). At early phases ( $< 15\text{d}$ ), the SYNOW-determined values from He I are found to be consistently higher by  $\sim 1000 \text{ km s}^{-1}$  from that determined using absorption minima, however, at phases 7d and 8d these values are consistent with that obtained from  $H\beta$  absorption minima. The  $H\alpha$  velocity is higher than  $v_{\text{phm}}$  by  $\sim 2000 \text{ km s}^{-1}$  at early phases and by  $\sim 1000 \text{ km s}^{-1}$  at later phases. As noted by TV12, we confirm that the line velocities of  $H\beta$  are in agreement with that of  $v_{\text{phm}}$  above  $10000 \text{ km s}^{-1}$ , while below this it is consistently higher than that determined using Fe II lines. The value of  $v_{\text{phm}}$  falls from  $2900 \text{ km s}^{-1}$  at 104d to  $1600 \text{ km s}^{-1}$  at 270d.

Fig. 18 shows the comparison of photospheric velocity of SN 2012aw with other well-studied SNe 1999em, 1999gi, 2004et, 1987A and 2005cs. For this comparison purpose the absorption trough velocities (average of Fe II lines at late phases and He I at early phases) have been used as the SYNOW-derived velocities are not available for all the SNe considered for comparison<sup>5</sup>. The velocity evolution of SN 2012aw is similar to the normal type IIP SNe 2004et, 1999em and 1999gi; though it is strikingly different than that of sub-luminous SN 2005cs and the type II-peculiar SN 1987A. The velocities of SN 2005cs are extremely less than SN 2012aw at all phases by  $\sim 3000 \text{ km s}^{-1}$ , whereas the profile of SN 1987A shows sharp decline in early phases ( $< 15\text{ days}$ ) and

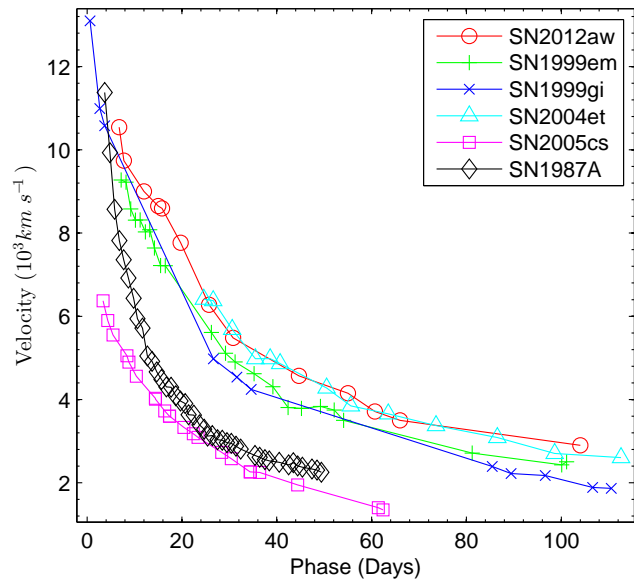


**Figure 18.** The evolution of photospheric velocity ( $v_{\text{ph}}$ ) of SN 2012aw is compared with other well-studied supernovae. The ( $v_{\text{ph}}$ ) plotted here are the absorption trough velocities (average of Fe II lines at late phases and He I at early phases).

comparatively slower decline in later phases. The entire photospheric velocity profile of SN 2012aw is identical to 2004et at all phases whereas it is consistently higher than that of SNe 1999em and 1999gi by  $\sim 600 \text{ km s}^{-1}$  at all phases. We note that while comparing Sc II 6247Å absorption velocities of SNe 2004et and 1999em, no difference is seen in velocity evolution (Maguire et al. 2010), however, velocities obtained using SYNOW model fits to the Fe II lines result in systematical higher velocities for SN 2004et (TV12). Similarly a comparison of expansion velocities of  $H\alpha$  and  $H\beta$  with other SNe indicate that these too are systematically higher than that observed for SNe 1999em and 1999gi; and are comparable with that observed for SN 2004et. For example, at phases 11d, 30d, and 50d respectively, the velocities of  $H\beta$  are  $11000$ ,  $7400$ , and  $5800 \text{ km s}^{-1}$  for SN 2004et (TV12);  $10000$ ,  $6600$ , and  $5000 \text{ km s}^{-1}$  for SN 2012aw (Table 6);  $8400$ ,  $5200$  and  $3500 \text{ km s}^{-1}$  for SN 1999em (TV12).

## 6 CHARACTERISTICS OF EXPLOSION

### 6.1 Explosion energy

The radiation-hydrodynamics simulations provided by Dessart et al. (2010) for core-collapse SNe generated artificially by driving a piston at the base of the envelope of a rotating and non-rotating red-supergiant progenitor stars, suggest that the  $v_{\text{ph}}$  at 15d after shock breakout is a good and simple indicator of the explosion energy ( $E_0$ ), no matter what the initial mass is. For non-rotating solar metallicity models with progenitor masses  $11\text{-}30M_{\odot}$ , a simulated plot of  $v_{\text{ph},15\text{d}}$  and the velocity at the outer edge of the oxygen-rich shell  $v_{\text{ej},\text{O}}$  (see Fig.4 in their paper) for different energy of explosion ranging from 0.1 to 3 foe ( $1 \text{ foe} = 10^{51} \text{ erg}$ ), indicate that the for SN 2012aw corresponding to the value of  $v_{\text{ph},15\text{d}} = 8650 \text{ km s}^{-1}$  (see Table 6), the value of  $E_0$  lies in the range

<sup>5</sup> Barring SN 1999em, taken from Leonard et al. (2002a), the velocities for all other comparison SNe are determined in this work using spectra available at SUSPECT <http://suspect.nhn.ou.edu>.

1-2 foe. The value of  $v_{\text{ph},15\text{d}}$  for SN 1999em is  $7650 \text{ km s}^{-1}$  whereas for SN 2004et it is  $8800 \text{ km s}^{-1}$  (TV12) and hence assuming similar nature of progenitor star, the strength of explosion for SN 2012aw should have been similar to SN 2004et but higher than that of SN 1999em. We note that a detailed radiation-hydrodynamic simulations of bolometric light-curves obtain value of  $E_0$  of  $1.3 \pm 0.3$  foe for SN 1999em (Utrobin 2007) and of  $2.3 \pm 0.3$  foe for SN 2004et (Utrobin & Chugai 2009).

Furthermore, the simulated models by Dessart et al. (2010) when combined with the width of observed nebular-phase O I 6300-6364Å line, can also be used to place an upper limit of the progenitor main-sequence mass. In nebular-phase spectra, an assessment of  $v_{\text{ej,O}}$  can be made by measuring half-width half-maxima (HWHM) of O I feature and for SN 2012aw it is found to be  $\sim 1340 \text{ km s}^{-1}$  at 270d and for comparison SNe 2004et, 1999em, 1987A, it is  $\sim 1300 \text{ km s}^{-1}$ ,  $\sim 1200 \text{ km s}^{-1}$  and  $\sim 1400 \text{ km s}^{-1}$  respectively (see Fig. 16). Hence the simulations for non-rotating models suggests an upper mass of  $15M_{\odot}$  for the progenitor star of SN 2012aw. Rotating models suggest lower-mass star. This upper mass limit for SN 2012aw is consistent with that determined by Kochanek et al. (2012) using data on pre-supernova stars and the stellar evolutionary models. We however note that the simulations of Dessart et al. (2010) assume no mixing of ejecta whereas the study of velocity distribution in line profile shapes of nebular lines by Maguire et al. (2012) indicate that mixing in ejecta is likely to have occurred in type IIP SNe. Consequently the width of [O I] lines may not represent true velocity of the oxygen-rich zones and hence the simulations-derived progenitor mass may be regarded as first hand estimates.

## 6.2 Mass of progenitor star

The mass of progenitor star can be estimated using nebular-phase emission line of O I 6300, 6364Å doublet as a detailed nucleosynthesis yields of stellar evolution/explosion models indicate that the core mass of metals in the inner ejecta is found to scale with the zero-age main-sequence mass of the progenitor (Woosley & Weaver 1995). Additionally, we also consider that in type II SNe, the nucleosynthesis yield is largely unaffected by late-time evolution of supernova ejecta. The mass of oxygen in type II SNe can be estimated by analysis of emission from the nebular phase [O I] doublet which is mainly powered by  $\gamma$ -ray depositions and more than half of the [O I] doublet luminosity during nebular phase is contributed by newly synthesized oxygen in the ejecta (Jerkstrand et al. 2012). Also, considering the fact that the SNe 2004et and 1987A have similar ejecta velocities and  $^{56}\text{Ni}$  masses; and the mass of oxygen for SNe 2004et and 1987A is modeled quite accurately and is available for comparison. We however note that the comparison with SN 2004et is more relevant as it is spectroscopically and photometrically similar to SN 2012aw. Following Elmhamdi et al. (2003), the luminosity of [O I] doublet can be written as:

$$L_{6300} = \eta \frac{M_{\text{O}}}{M_{\text{ex}}} L(^{56}\text{Co})$$

where  $M_{\text{O}}$  is the mass of oxygen,  $M_{\text{ex}}$  is the ‘excited’ oxygen mass in which bulk of decay energy is deposited,  $\eta$  is the efficiency of transformation of decay energy deposited into

[O I] doublet radiation and  $L(^{56}\text{Co})$  is the luminosity of  $^{56}\text{Co}$  which is directly proportional to the mass of ejected  $^{56}\text{Ni}$ .

The O I luminosity of  $\sim 1.36 \times 10^{39} \text{ erg s}^{-1}$  is obtained for SN 2012aw by integrating the flux within local minima (6214 – 6471Å) and subtracting the local continuum in that region. Similarly a value of  $\sim 1.64 \times 10^{39} \text{ erg s}^{-1}$  is estimated for SNe 2004et at 270d by interpolating the value using 259d and 301d spectra taken from Sahu et al. (2006). Assuming that in both SNe 2004et and 2012aw,  $\eta$  and  $M_{\text{ex}}$  are similar and given 0.83 times lower luminosity of [O I] doublet in SN 2012aw at 270d and equal  $^{56}\text{Ni}$  mass (§4.4), we derive a rough estimate of oxygen in SN 2012aw to be a factor 0.83 lower than in SN 2004et. Considering the oxygen mass of SN 2004et as  $0.8 M_{\odot}$ , estimated using spectral modelling of nebular phase (140d to 700d) spectra from ultraviolet to mid-infrared (Jerkstrand et al. 2012), the mass for SN 2012aw translates to be  $0.66 M_{\odot}$  and using nucleosynthesis yield computations in massive stars (11-40  $M_{\odot}$ ) by Woosley & Weaver (1995) corresponds to the main-sequence solar metallicity stellar mass of 14-15  $M_{\odot}$ .

The comparison with O I luminosity of SN 1987A (a value of  $\sim 2.1 \times 10^{39} \text{ erg s}^{-1}$  is estimated by interpolating values obtained at 197d and 338d using spectrum taken from Pun et al. (1995)) with SN 2012aw indicate that mass of oxygen in SN 2012aw to be a factor 0.84 lower than in SN 2004et. Considering the oxygen mass determinations of SN 1987A in range 1.2-1.5  $M_{\odot}$  (Li & McCray 1992; Chugai 1994; Kozma & Fransson 1998), the mass range for SN 2012aw translates to be 1.0-1.26  $M_{\odot}$  and using nucleosynthesis computations this corresponds to the main-sequence solar metallicity stellar mass of 17-19  $M_{\odot}$  (Woosley & Weaver 1995).

The minimum mass of oxygen can also be obtained independently using the equation (Uomoto 1986):

$$M_{\text{O I}} = 10^8 F_{\text{O I}} D^2 e^{2.28/T_4}$$

where  $F_{\text{O I}}$  is the O I doublet flux in units of  $\text{erg s}^{-1}$ ,  $D$  is the distance to the SN in units of Mpc and  $T_4$  is the temperature in units of  $10^4 \text{ K}$ . From Liu & Dalgarno (1995), the O temperature of SN 1987A at 300 days was  $\sim 4200 \text{ K}$ . Assuming a similar O temperature for SN 2012aw at a comparable epoch, the oxygen mass for SN 2012aw was calculated for temperatures in the range 3500–4500 K as  $0.18 - 0.77 M_{\odot}$  with the corresponding minimum main-sequence masses in the range 11-16  $M_{\odot}$ .

## 6.3 Explosion parameters

Accurate estimates of explosion parameters of type IIP SNe require detailed hydrodynamical modelling of their bolometric light-curve (e.g. Bersten et al. 2011, references therein) which is beyond the scope of this paper, however the analytical relations connecting the observed parameters (viz. the duration of plateau  $\Delta t_{\text{p}}$ , the mid-plateau absolute magnitude  $M_{\text{p}}^{\text{V}}$  magnitude and mid-plateau photospheric velocity  $v_{\text{p}}$ ) with physical parameters of the explosion (viz. the energy of the explosion  $E_0$ , the radius of progenitor star  $R_0$  and the mass of the ejected matter  $M_{\text{ej}}$ ) do exist (Arnett 1980). Litvinova & Nadezhin (1983, 1985, LN85) made numerical calibration of these relations for a wide range of observables using a grid of hydrodynamical models for different values of  $E_0$ ,  $R_0$  and  $M_{\text{ej}}$ . The applicability of such

**Table 7.** Explosion parameters of well-studied type IIP SNe. The references for the adopted time of explosion ( $t_0$ ), distance ( $D$ ) and reddening  $E(B - V)$  are given in Fig. 5. See §6.3 for further details.

Name	$t_0$ (2450000+)	$\Delta t_p$ (day)	$t_p$ (day)	$M_V^P$ (mag)	$v_p$ (km s $^{-1}$ )	$E_0$ ( $\times 10^{50}$ erg)	$M_{ej}$ ( $M_\odot$ )	$R_0$ ( $R_\odot$ )
SN 1999em	1475.6	$92 \pm 8$	$55 \pm 4$	$-16.69 \pm 0.01$	$3512 \pm 122$	$7 \pm 2$	$11 \pm 3$	$399 \pm 54$
SN 1999gi	1522.3	$97 \pm 8$	$58 \pm 4$	$-16.26 \pm 0.02$	$2746 \pm 217$	$4 \pm 1$	$10 \pm 3$	$421 \pm 99$
SN 2004et	3270.5	$87 \pm 8$	$63 \pm 4$	$-17.01 \pm 0.03$	$3630 \pm 142$	$6 \pm 2$	$9 \pm 2$	$591 \pm 90$
SN 2012aw	6002.6	$96 \pm 11$	$57 \pm 6$	$-16.67 \pm 0.03$	$3631 \pm 200$	$9 \pm 3$	$14 \pm 5$	$337 \pm 67$

a relation have been questioned as the ejected masses derived using LN85 relations for large set of IIP SNe (14–56  $M_\odot$  by Hamuy 2003); (10–30  $M_\odot$  by Nadyozhin 2003); are consistently higher than that obtained using direct pre-SN imaging (6–15  $M_\odot$  by Smartt et al. 2009). Some of the problems lie in the lack of good quality data, simplified physical assumptions and non-inclusion of nickel heating effects (e.g. see Bersten et al. 2011), however, these relations are still useful in comparing the relative explosion properties of IIP SNe.

For the sake of estimating observed parameters for SN 2012aw and comparing with other SNe, having similar light-curve/spectra behavior, in a consistent manner, we consider nearby normal type IIP SNe 1999em, 1999gi and 2004et for which the distances, reddening and time of explosions are known quite accurately and all of these have good photometric and spectroscopic observations during plateau phase. The value of  $\Delta t_p$  to be determined using  $M_V$  light-curve (see Fig. 5) in a manner described by Nadyozhin (2003) is non trivial, however, a plateau duration of  $\sim 100$  days is clearly apparent for all the four SNe. As noted in §4.1, the V-band light-curve of sample SNe peaks between 10–16d post explosion and show a slow linear decline until  $\sim 110$ d, we have therefore fitted a straight line to the linear part of the plateau to estimate the phases at which the slope changes significantly by including two consecutive points at the ends. The value of  $\Delta t_p$  determined in this way and the phase  $t_p$  corresponding to mid-point are given in Table 7. Furthermore, at  $t_p$ , we obtain both, the value of  $M_V^P$  by linear interpolation (data from Fig. 5) and the value of  $v_p$  by third order polynomial interpolation of  $v_{pha}$  values shown in Fig. 18, which were determined by absorption minima to Fe II lines. The explosion parameters determined in this way is listed in Table 7 and it can be seen that the properties of SN 2012aw is very much similar to SNe 1999gi, 1999em and 2004et.

The value of  $E_0$  is close to the standard energy of SNe explosion ( $\sim 10^{51}$  erg) and the pre-supernova radius is consistent with that of Galactic red supergiant stars measured observationally by Levesque et al. (2005). The value of  $M_{ej}$  lies in the range 9–14  $M_\odot$  and accounting for a total of  $2M_\odot$  including mass of neutron star (a possible endpoint of IIP SNe) and the mass loss during red supergiant phase, this corresponds to a main sequence mass of 11–16  $M_\odot$ . It is noted that using Sc II 4670Å line for the photospheric velocities in our computation provides lower values of ejected masses. These values are consistent with the values determined using direct imaging of pre-supernova stars (Smartt et al. 2009). Furthermore, it is seen that all these SNe have similar properties in terms of explosion energy, ejected mass and the

radius of pre-supernova star and considering uncertainty in estimating  $\Delta t_p$  and  $v_p$ , it is difficult to find any trend in their relative explosion parameters, and we need a larger sample of nearby IIP SNe having good-quality data and a uniform approach to verify the applicability of analytical relations. For example, we note that using the LN85 relations, Maguire et al. (2010) derived the value of  $M_{ej}$  for SNe 1999em, 1999gi and 2004et in the range 14–21  $M_\odot$  and they employed plateau duration in the range 110–120 days and the photospheric velocity derived from Sc II 6246Å line.

## 7 CONCLUSIONS

We present new *UBVRI* photometric and low resolution spectroscopic observations of a supernova event SN 2012aw which occurred in the outskirts of a nearby ( $9.9 \pm 0.1$  Mpc) galaxy M95. The time of explosion is constrained with an accuracy of a day and the position of SN in the galaxy is consistent with being located in a solar metallicity region. The photometric observations are presented at 45 phases during 4d to 269d while the low-resolution (6–12Å) spectroscopic observations are presented at 14 phases during 7d to 270d. Employing the high-resolution spectrum of Na I D region and the early time photometric spectral energy distribution, the value of  $E(B - V)$  is constrained quite accurately to be  $0.07 \pm 0.01$  mag.

The light-curve characteristics of apparent magnitudes, colors and the bolometric luminosity is found to have striking similarity with the archetypal IIP SNe 1999em, 1999gi and 2004et; all showing plateau duration of about 100 days. For all these SNe, the light-curve in V-band rises to a peak between 10–16d post explosion and then follows slow decline during plateau-phase. However, for SN 2012aw our early time observations clearly detect minima in the light-curve of V, R and I bands near 32 days after explosion and this we suggest to be an observational evidence seen for the first time in any type IIP SNe, for the emergence of flux due to onset of recombination phase. The value of mid-plateau  $M_V$  is  $-16.67 \pm 0.04$  for SN 2012aw lies in between the bright IIP SNe ( $\sim -18$  mag; e.g. 2007od, 2009bw) and the subluminous IIP SNe ( $\sim -15$  mag; e.g. 2005cs, 1997D). Employing nebular-phase bolometric luminosity, we estimate mass of  $^{56}\text{Ni}$  to be  $0.06 \pm 0.01$ , similar to the SNe 1999em, 2004et and 1987A.

The presence and evolution of prominent optical spectral features show striking similarity with the IIP SNe 1999em, 1999gi and 2004et. We have identified and studied the evolution of spectral features using SYNOW modelling. Similar to SNe 1999em, and 1999gi, two peculiar high-velocity components associated with the regular H $\beta$

and He I P-Cygni features are seen in the early (7 & 8d) spectra, indicating early interaction of ejecta with the circumstellar material. However, these absorption features are consistent with being reproduced by invoking N II lines in the SYNOW modelling. During 55-104d, the absorption profiles of H $\beta$  and H $\alpha$  is broadened and it only fit by invoking high-velocity components showing signs of ejecta interaction with CSM during late plateau phase. We note that interaction scenario is consistent with the detection of SN 2012aw in X-rays (0.1-10 keV) during 4-6d (Immler & Brown 2012) and at 21 GHz radio observations during 8-14d (Stockdale et al. 2012; Yadav et al. 2012)

The velocity of H $\alpha$  and [O I] doublet line-emitting regions in the nebular phase spectrum at 270d is found to be similar to that observed for SNe 1999em and 2004et; and the line profile shapes are consistent with being originated from spherically symmetric regions, showing no signs of dust formation.

The value and evolution of photospheric velocity as derived using Fe II lines is found to be similar to SN 2004et, but about  $\sim 600 \text{ km s}^{-1}$  higher than that of SNe 1999em and 1999gi at similar epochs. This trend was more apparent in the line velocities of H $\alpha$  and H $\beta$ . The comparison of photospheric velocity at 15d with that derived using radiation-hydrodynamics simulations of IIP SNe by Dessart et al. (2010) indicate that the energy of explosion is about  $1 - 2 \times 10^{51}$  erg and this coupled with the velocity of [O I] line suggests an upper mass limit of  $15M_{\odot}$  for a non-rotating solar metallicity progenitor star. We further constrain, the progenitor mass by comparing [O I] emission luminosity with the SNe 2004et and 1987A and we find that the core of oxygen mass was smaller than that of SNe 2004et and 1987A; and assuming similar physical conditions, we derive mass of progenitor star about 14-15  $M_{\odot}$ .

We have also estimated explosion parameters using analytical relations of LN85 for SNe 1999gi, 1999em, 2004et and 2012aw; all having good coverage of photometric and spectroscopic data during plateau phase, in a consistent manner. We find no trend in relative parameters but ensemble parameters are found to be consistent with that expected for a normal luminosity IIP SNe, i.e., the explosion energy is consistent with  $1 \times 10^{51}$  erg, the pre-supernova radius is similar to what is expected from a red-supergiant star and the mass of progenitor lies between 11-16  $M_{\odot}$ .

SN 2012aw along with type IIP SNe 1999gi, 1999em and 2004et forms a golden sample to test results from radiation hydrodynamical simulations.

## ACKNOWLEDGMENTS

We thank all the observers at Aryabhata Research Institute of Observational Sciences (ARIES) who provided their valuable time and support for the observations of this event. We are thankful to the observing staffs and technical assistants of ARIES 1.3-m Devasthal telescope and we also express our thanks to 2-m IGO, 2-m HCT telescope staffs for their kind cooperation in observation of SN 2012aw. We gratefully acknowledge the services of the NASA ADS and NED databases and also the online supernova spectrum archive (SUSPECT) which are used to access data and references in this paper. We thank K. Maguire for providing late spec-

troscopic data of SN 2004et. The authors would also like to thank the anonymous referee for the comments and suggestions which helped in improvement of this manuscript.

## REFERENCES

- Arcavi I., Gal-Yam A., Cenko S. B., et al., 2012, ApJL, 756, L30
- Arnett D., 1996, *Supernovae and Nucleosynthesis: An Investigation of the History of Matter from the Big Bang to the Present*
- Arnett W. D., 1980, ApJ, 237, 541
- Asplund M., Grevesse N., Sauval A. J., Scott P., 2009, ARA&A, 47, 481
- Barbon R., Benetti S., Rosino L., Cappellaro E., Turatto M., 1990, A&A, 237, 79
- Baron E., Branch D., Hauschildt P. H., et al., 2000, ApJ, 545, 444
- Baron E., Nugent P. E., Branch D., Hauschildt P. H., 2004, ApJL, 616, L91
- Bayless A. J., Pritchard T. A., Roming P. W. A., et al., 2013, ApJL, 764, L13
- Bersten M. C., Benvenuto O., Hamuy M., 2011, ApJ, 729, 61
- Bose S., Kumar B., 2013, IAUS, 296, (in press)
- Branch D., Benetti S., Kasen D., et al., 2002, ApJ, 566, 1005
- Burrows A., 2013, *Reviews of Modern Physics*, 85, 245
- Cardelli J. A., Clayton G. C., Mathis J. S., 1989, ApJ, 345, 245
- Chakraborty P., Das H. K., Tandon S. N., 2005, *Bulletin of the Astronomical Society of India*, 33, 513
- Chugai N. N., 1988, *Soviet Astronomy Letters*, 14, 334
- Chugai N. N., 1994, ApJL, 428, L17
- Cowen D. F., Franckowiak A., Kowalski M., 2010, *Astroparticle Physics*, 33, 19
- Dessart L., Hillier D. J., 2005a, A&A, 437, 667
- Dessart L., Hillier D. J., 2005b, in *The Fate of the Most Massive Stars*, edited by R. Humphreys, K. Stanek, vol. 332 of *Astronomical Society of the Pacific Conference Series*, 415
- Dessart L., Hillier D. J., 2006, A&A, 447, 691
- Dessart L., Livne E., Waldman R., 2010, MNRAS, 408, 827
- Elmhamdi A., Danziger I. J., Chugai N., et al., 2003, MNRAS, 338, 939
- Fagotti P., Dimai A., Quadri U., et al., 2012, *Central Bureau Electronic Telegrams*, 3054, 1
- Filippenko A. V., 1997, ARA&A, 35, 309
- Fisher A., Branch D., Hatano K., Baron E., 1999, MNRAS, 304, 67
- Fisher A., Branch D., Nugent P., Baron E., 1997, ApJL, 481, L89
- Fraser M., Ergon M., Eldridge J. J., et al., 2011, MNRAS, 417, 1417
- Fraser M., Maund J. R., Smartt S. J., et al., 2012, ApJL, 759, L13
- Freedman W. L., Madore B. F., Gibson B. K., et al., 2001, ApJ, 553, 47
- Fukugita M., Shimasaku K., Ichikawa T., 1995, PASP, 107, 945

- Gandhi P., Yamanaka M., Tanaka M., et al., 2013, *ApJ*, 767, 166
- Gupta R., Burse B., Das H. K., et al., 2002, *BASI*, 30, 745
- Hamuy M., 2003, *ApJ*, 582, 905
- Hamuy M., Suntzeff N. B., 1990, *AJ*, 99, 1146
- Hamuy M., Suntzeff N. B., Heathcote S. R., Walker A. R., Gigoux P., Phillips M. M., 1994, *PASP*, 106, 566
- Hanuschik R. W., Dachs J., 1987, *A&A*, 182, L29
- Heger A., Fryer C. L., Woosley S. E., Langer N., Hartmann D. H., 2003, *ApJ*, 591, 288
- Henden A., Krajić T., Munari U., 2012, *Information Bulletin on Variable Stars*, 6024, 1
- Horne K., 1986, *PASP*, 98, 609
- Immmer S., Brown P. J., 2012, *The Astronomer's Telegram*, 3995, 1
- Inserra C., Baron E., Turatto M., 2012a, *MNRAS*, 422, 1178
- Inserra C., Turatto M., Pastorello A., et al., 2011, *MNRAS*, 417, 261
- Inserra C., Turatto M., Pastorello A., et al., 2012b, *MNRAS*, 422, 1122
- Itoh R., Ui T., Yamanaka M., 2012, *Central Bureau Electronic Telegrams*, 3054, 2
- Janka H.-T., 2012, *Annual Review of Nuclear and Particle Science*, 62, 407
- Jeffery D. J., Branch D., 1990, in *Supernovae, Jerusalem Winter School for Theoretical Physics*, edited by J. C. Wheeler, T. Piran, S. Weinberg, 149
- Jerkstrand A., Fransson C., Maguire K., Smartt S., Ergon M., Spyromilio J., 2012, *A&A*, 546, A28
- Jordi K., Grebel E. K., Ammon K., 2006, *A&A*, 460, 339
- Kasen D., Woosley S. E., 2009, *ApJ*, 703, 2205
- Kochanek C. S., Khan R., Dai X., 2012, *ApJ*, 759, 20
- Kozma C., Fransson C., 1998, *ApJ*, 497, 431
- Landolt A. U., 2009, *AJ*, 137, 4186
- Leonard D. C., Filippenko A. V., Gates E. L., et al., 2002a, *PASP*, 114, 35
- Leonard D. C., Filippenko A. V., Li W., et al., 2002b, *AJ*, 124, 2490
- Leonard D. C., Pignata G., Dessart L., et al., 2012, *The Astronomer's Telegram*, 4033, 1
- Levesque E. M., Massey P., Olsen K. A. G., et al., 2005, *ApJ*, 628, 973
- Li H., McCray R., 1992, *ApJ*, 387, 309
- Litvinova I. I., Nadezhin D. K., 1983, *Ap&SS*, 89, 89
- Litvinova I. Y., Nadezhin D. K., 1985, *Soviet Astronomy Letters*, 11, 145
- Liu W., Dalgarno A., 1995, *ApJ*, 454, 472
- Maguire K., Di Carlo E., Smartt S. J., et al., 2010, *MNRAS*, 404, 981
- Maguire K., Jerkstrand A., Smartt S. J., et al., 2012, *MNRAS*, 420, 3451
- Misra K., Pooley D., Chandra P., et al., 2007, *MNRAS*, 381, 280
- Munari U., Vagnozzi A., Castellani F., 2012, *Central Bureau Electronic Telegrams*, 3054, 3
- Nadyozhin D. K., 2003, *MNRAS*, 346, 97
- Oke J. B., 1990, *AJ*, 99, 1621
- Pastorello A., Pumo M. L., Navasardyan H., et al., 2012, *A&A*, 537, A141
- Pastorello A., Turatto M., Benetti S., et al., 2002, *MNRAS*, 333, 27
- Pastorello A., Valenti S., Zampieri L., et al., 2009, *MNRAS*, 394, 2266
- Pastorello A., Zampieri L., Turatto M., et al., 2004, *MNRAS*, 347, 74
- Patat F., Barbon R., Cappellaro E., Turatto M., 1994, *A&A*, 282, 731
- Pilyugin L. S., Thuan T. X., Vílchez J. M., 2006, *MNRAS*, 367, 1139
- Poznanski D., Ganeshalingam M., Silverman J. M., Filippenko A. V., 2011, *MNRAS*, 415, L81
- Poznanski D., Nugent P. E., Ofek E. O., Gal-Yam A., Kasliwal M. M., 2012a, *The Astronomer's Telegram*, 3996, 1
- Poznanski D., Prochaska J. X., Bloom J. S., 2012b, *MNRAS*, 426, 1465
- Pun C. S. J., Kirshner R. P., Sonneborn G., et al., 1995, *ApJS*, 99, 223
- Quimby R. M., Wheeler J. C., Höflich P., Akerlof C. W., Brown P. J., Rykoff E. S., 2007, *ApJ*, 666, 1093
- Roy R., Kumar B., Benetti S., et al., 2011, *ApJ*, 736, 76
- Russell D. G., 2002, *ApJ*, 565, 681
- Sagar R., Kumar B., Omar A., 2013, *ArXiv e-prints*
- Sagar R., Kumar B., Omar A., Joshi Y. C., 2012, in *Astronomical Society of India Conference Series*, vol. 4 of *Astronomical Society of India Conference Series*, 173
- Sahu D. K., Anupama G. C., Sridivya S., Muneer S., 2006, *MNRAS*, 372, 1315
- Schlegel D. J., Finkbeiner D. P., Davis M., 1998, *ApJ*, 500, 525
- Siviero A., Tomasella L., Pastorello A., et al., 2012, *Central Bureau Electronic Telegrams*, 3054, 4
- Smartt S. J., Eldridge J. J., Crockett R. M., Maund J. R., 2009, *MNRAS*, 395, 1409
- Stalin C. S., Hegde M., Sahu D. K., et al., 2008, *Bulletin of the Astronomical Society of India*, 36, 111
- Stetson P. B., 1987, *PASP*, 99, 191
- Stetson P. B., 1992, *J. R. Astron. Soc. Canada*, 86, 71
- Stockdale C. J., Ryder S. D., Van Dyk S. D., et al., 2012, *The Astronomer's Telegram*, 4012, 1
- Takáts K., Vinkó J., 2012, *MNRAS*, 419, 2783
- Tsvetkov D. Y., Goranskij V., Pavlyuk N., 2008, *Peremennye Zvezdy*, 28, 8
- Turatto M., Benetti S., Cappellaro E., 2003, in *From Twilight to Highlight: The Physics of Supernovae*, edited by W. Hillebrandt, B. Leibundgut, 200
- Uomoto A., 1986, *ApJL*, 310, L35
- Utrobin V. P., 2007, *A&A*, 461, 233
- Utrobin V. P., Chugai N. N., 2009, *A&A*, 506, 829
- Utrobin V. P., Chugai N. N., 2011, *A&A*, 532, A100
- van Dokkum P. G., 2001, *PASP*, 113, 1420
- Van Dyk S. D., Cenko S. B., Poznanski D., et al., 2012, *ApJ*, 756, 131
- Vollmann K., Eversberg T., 2006, *Astronomische Nachrichten*, 327, 862
- Woosley S. E., Weaver T. A., 1995, *ApJS*, 101, 181
- Yadav N., Chakraborti S., Ray A., 2012, *The Astronomer's Telegram*, 4010, 1